Fabrication and Characterization of Conducting Polymer Microwires

by

Miguel Angel Sáez

S.B. Mechanical Engineering
Massachusetts Institute of Technology, 2007

Submitted to the Department of Mechanical Engineering
in partial fulfillment of the requirements for the degree of

Master of Science in Mechanical Engineering

at the

MASSACHUSETTS INSTITUTE OF TECHNOLOGY

September 2009

Author ....
Department of Mechanical Engineering
July 29, 2009

Certified by ....
Ian W. Hunter
Hatsopolous Professor of Mechanical Engineering
Thesis Supervisor

Accepted by ....
David E. Hardt
Chairman, Department Committee on Graduate Students

Fabrication and Characterization of Conducting Polymer Microwires

by

Miguel Angel Sáez

Submitted to the Department of Mechanical Engineering
on July 29, 2009, in partial fulfillment of the
requirements for the degree of
Master of Science in Mechanical Engineering

Abstract

Flexible microwires fabricated from conducting polymers have a wide range of potential applications, including smart textiles that incorporate sensing, actuation, and data processing. The development of garments that integrate these functionalities over wide areas (i.e. the human body) requires the production of long, highly conductive, and mechanically robust fibers or microwires. This thesis describes the development of a microwire slicing instrument capable of producing conducting polymer wires with widths as small as a few micrometers and lengths ranging from tens of millimeters to meters. To ensure high conductivity and robustness, the wires are sliced from thin polypyrrole films electrodeposited onto a glassy carbon crucible. Extensive testing was conducted to determine the optimal cutting parameters for producing long, fine wires with cleanly cut edges. This versatile fabrication process has been used to produce free-standing microwires with cross-sections of 2 μm $\times$ 3 μm, 20 μm $\times$ 20 μm, and 100 μm $\times$ 20 μm with lengths of 15 mm, 460 mm, and 1,200 mm, respectively. An electrochemical dynamic mechanical analyzer was used to measure the static and dynamic tensile properties, the strain-resistance relationship, and the electrochemical actuation performance of the microwires. The measured gage factors ranged from 0.4 to 0.7 and are suitable for strain sensing applications. Strains and forces of up to 2.9% and 2.3 mN were recorded during electrochemical actuation in $BMIMPF_6$. These monofilament microwires may be spun into yarns or braided into 2- and 3- dimensional structures for use as actuators, sensors, micro antennas, and electrical interconnects in smart fabrics.

Thesis Supervisor: Ian W. Hunter
Title: Hatsopolous Professor of Mechanical Engineering

Acknowledgments

Working in the BioInstrumentation Lab for the past three years as both an undergraduate and master's student has been an incredible learning experience. My time in the Lab has allowed me to make use of my knowledge of science and engineering in meaningful ways. First and foremost, I would like to thank Professor Ian Hunter for his support and for providing me with the opportunity to conduct my thesis research in the Lab. Senior Lab members Priam Pillai, Tim Fofonoff and Brian Ruddy have shared with me their extensive knowledge of mechanical design and conducting polymers. Their advice, guidance and support were critical to the success of this work. I would also like to thank my BioInstrumetation Lab colleagues Dr. Cathy Hogan, Brian Hemond, Scott McEuen, Adam Wahab, Jessica Galie, Ellen Chen, Jean Chang, Kerri Keng and Eli Paster. I am honored to have had the privilege of working with such a talented and diverse group of researchers. Thanks also to my UROP Lauren Montemayor for her excellent work helping me with the imaging and tensile testing of the polymer microwires. I would also like to acknowledge the National Science Foundation, the Institute for Soldier Nanotechnologies, and the Intelligence Advanced Research Projects Activity for providing funding for this work for the past two years.

I would like to thank Anirban Mazumdar for his awesome friendship during the past years and for helping rekindle my love for basketball. A very special thank you goes out to my best friend and future M.D. Tania Sierra for all her love and support throughout the years. Her passion and dedication to her dreams inspire me.

Por supuesto, le doy gracias a mis queridos padres, Angel y Janet, por todo el amor y apoyo que me han dado desde pequeño. Les agradezco con todo mi corazón lo que han hecho y sacrificado para darme la oportunidad de estudiar ingeniería en MIT. También le doy gracias a mi hermano Angel Omar por su amor y apoyo. Es mi deseo que podamos ayudarnos uno al otro y que siempre nos mantengamos unidos, en las buenas y en las malas. Finalmente, muchas gracias a Abuela Joahnie y al resto de mi familia por todo su amor y cariño a través de los años.

Contents

List of Figures

List of Tables

Chapter 1

Introduction

Flexible microwires fabricated from conducting polymers have a wide range of possible applications including smart textiles, high fidelity neural recording, micro antennas, and flexible polymer-based electronics. Smart textiles that incorporate sensing, information processing and actuation in a flexible platform have garnered increased interest in recent years. Advances in textile nanotechnologies are enabling the integration of these various functionalities into wearable electronic systems while maintaining the look and feel of traditional fabrics [13]. With demand for smart textiles growing in industries ranging from military and security to healthcare and fitness, the market for these technologies is expected to reach $115 billion by 2012 [1].

Conducting polymers such as polypyrrole and polyaniline are unique among the materials currently studied for use in smart textiles because of their ability to act as both sensors and actuators. These materials sense by changing their electrical properties in response to external stimuli, and are capable of generating significant stresses at strains comparable to mammalian skeletal muscle [28]. Early conducting fabrics were typically created by depositing polypyrrole onto traditional materials such as nylon [29, 40]. Researchers are now working to produce all-polymer fibers or microwires which can be spun into yarns and used to create a wide range of fabric structures.

Various research groups have used electrospinning and wet spinning techniques to produce polypyrrole fibers, but these methods typically result in materials with

poor conductivities [11, 16]. This thesis proposes a completely different approach which involves slicing long, fine microwires from a highly conductive polypyrrole thin film electrodeposited onto a glassy carbon crucible. It describes the development and testing of a computer-controlled, four-axis microwire slicing instrument capable of producing PPy microwires with widths as small as a few microns and lengths ranging from tens of millimeters to meters. The characterization of the electrical, mechanical and electrochemical properties of the produced microwires is also presented.

Chapter 2

Conducting Polymers

Conducting polymers are a unique class of materials that exhibit the electrical properties of metals while retaining the mechanical properties of traditional engineering plastics. They form part of a group of ionically driven polymers that have the ability to undergo mechanical deformations that mimic the performance of muscle. The following sections provide an overview of the properties of conducting polymers, with a focus on polypyrrole (PPy), and a description of its actuation mechanism. Also included is a detailed description of the polymer synthesis technique used by Professor Ian Hunter's Group at MIT to produce the highly conductive and mechanically robust PPy films used in this work.

2.1 History and General Properties

The production of conducting polymers dates back to the mid 19th century when Letheby first reported the anodic oxidation of aniline [24]. Despite this and other early efforts, conducting polymers remained poorly understood and their properties were not adequately characterized until the 1970's [18, 21]. Polyacetylene, the first well-characterized conducting polymer, was shown to be electrically conductive in 1977 [10]. This work was recognized with the 2000 Nobel Prize in Chemistry [17]. Since then, numerous other conducting polymers have been synthesized and described [42].

In general, conducting polymers are differentiated from traditional polymers by a conjugated backbone structure containing alternating single and double carbon bonds capable of forming a delocalized electron cloud. These long backbone structures are not fully conjugated and are electronically characterized by a band gap. Thus, most undoped conducting polymers are essentially semiconductors [36]. Their conductivity can be greatly enhanced by adding dopants via oxidation or reduction and metallic conductivities can be achieved under certain conditions [44]. The backbone structure is very stiff and prevents conducting polymers from melting or dissolving in solvents, making them difficult to process. Also, conducting polymers generally exhibit high chemical sensitivity and are highly active in oxidation and reduction reactions occurring in both electrochemical and chemical processes.

Current conducting polymer research centers on a number of well-characterized varieties noted for their high conductivity and stability. The Hunter group has focused its efforts on a small number of these materials, placing special emphasis on the characterization and development of PPy for use as a sensor and actuator. The chemical structure of PPy and other commonly used conducting polymers can be seen in Figure 2-1.

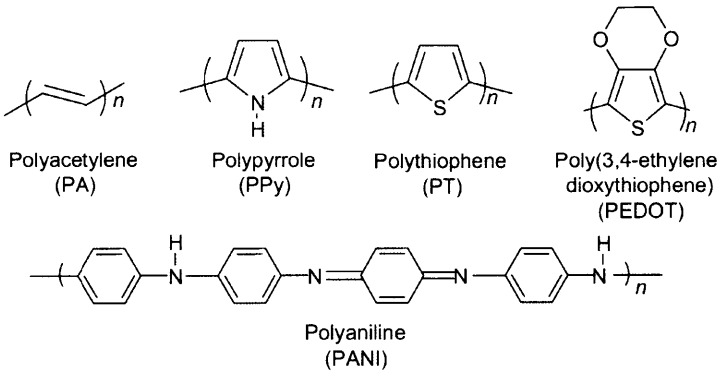

Figure 2-1: A schematic of the bond structures of common conducting polymers in the undoped form (Taken from [19])

PPy attracts strong interest because of its high conductivity and stability in ambient conditions. It is often described as *artificial muscle* due to the ability of PPy films to undergo changes in volume under electrochemical stimulus via ion diffusion,

achieving strains comparable to mammalian skeletal muscle [28]. The Hunter group typically produces free standing black films 2 μm to 50 μm thick with as-deposited conductivities of 10^4 S/m to 10^5 S/m. These films are mechanically robust, and their elastic modulus and yield strength are about 1 GPa and 40 MPa, respectively [2, 33]. Methods for the processing of PPy films following deposition are limited because of the strong interchain interactions. The films are generally insoluble and decompose at temperatures above 200°C. Hence, processing is limited to cutting, which can be done using blades, a carbon-dioxide laser or by electric discharge machining. A number of soluble PPy systems have been developed by various research groups for the production of films and fibers, but typically result in materials with poor conductivity [16].

2.2 Actuation Mechanism

A conducting polymer must be incorporated into an electrochemical cell in order to achieve functional actuation. The cell consists of a PPy film or wire acting as the working electrode and a counter electrode made up of a non-reactive conducting material, such as stainless steel or glassy carbon. Both electrodes are suspended in an electrolyte solution which provides dopant ions and the medium through which the ions move.

When a potential is applied between the PPy and the counter electrode, an electrostatic field is established which creates a capacitive double layer at the polymer/electrolyte interface. The resulting reduction or oxidation of the PPy causes ions to move in and out of the polymer matrix in order to balance the charge. This ion diffusion causes the PPy to swell or contract, and therefore generate stresses and strains. In practice, the solution cation-anion pair is chosen such that the actuation is dominated by the smaller, more mobile ion, which must still be large enough to produce useful changes in volume. The electrolyte solution used in this work was 1-Butyl-3-methylimidazolium hexafluorophosphate ($BMIMPF_6$), which produces a response in which the $BMIM^+$ cation dominates the actuation and causes the PPy

to swell during reduction, as depicted in Figure 2-2 [35].

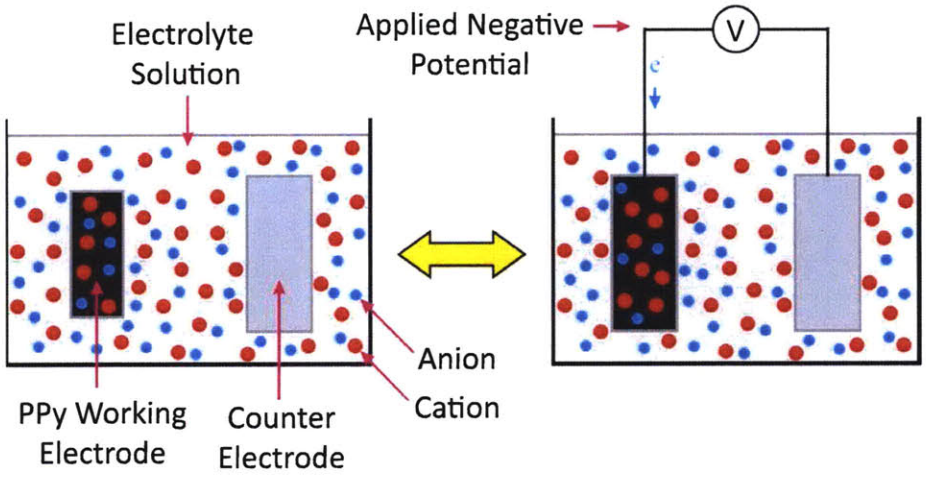

Figure 2-2: Schematic of a basic electrochemical cell used to change the oxidative state of a conducting polymer. When a voltage is applied, the polymer's volume changes as ions diffuse in and out of the material. (Taken from [14])

The electrical and mechanical behavior of a PPy actuator can be described using the diffusive-elastic metal (DEM) model developed by John Madden [28]. The model is in the form of the polymer admittance and is given by the equation

$$Y(s) = \frac{s}{R} \cdot \frac{\frac{\sqrt{D}}{\delta} \cdot tanh\left(\frac{a}{2}\sqrt{\frac{s}{D}}\right) + \sqrt{s}}{\frac{\sqrt{s}}{RC} + s^{3/2} + \frac{\sqrt{D}}{\delta} \cdot s \cdot tanh\left(\frac{a}{2}\sqrt{\frac{s}{D}}\right)}, \tag{2.1}$$

where D is the diffusion coefficient, δ is the thickness of the capacitive double layer, C is the double layer capacitance, R is the polymer reistance, a is the polymer thickness, and s is the Laplace variable. Dimensional analysis of Equation 2.1 yields three time constants that govern the time response of the polymer. τ_D is the time constant related to ion diffusion in the polymer, τ_{RC} is related to the charging of the double layer, and τ_{DDL} is related to ion diffusion through the double layer. They are given by

$$\begin{aligned} \tau_D &= \frac{a^2}{4D}, \\ \tau_{RC} &= RC, and \end{aligned} \tag{2.2}$$

$$\tau_{DDL} = \frac{\delta^2}{D}.$$

The rate of ion diffusion through the polymer (τ_D) dominates the response, and controls the charging rate of the polymer, which is directly related to the actuation rate.

A key assumption made in the DEM model is that a uniform electrical potential exists throughout the polymer film. This assumption is not valid for high aspect ratio polymer actuators with large resistances, such as long, thin films and microwires. The resistance causes a voltage drop along the length of the actuator, which reduces the concentration of ions at the double layer, and thus decreases the charging rate and the actuation rate of the polymer. Past research conducted by Tim Fofonoff of the Hunter Group demonstrated that adding a fine gold layer onto a long strip of PPy film reduced the ohmic voltage drop, and thus significantly improved the rate of actuation [14]. Fofonoff's results were confirmed by actuation tests of gold-backed PPy microwires conducted as part of this work. The results of these tests are presented and discussed in Section 6.5.

2.3 Synthesis of Polypyrrole Films

The PPy films used in this work were fabricated using an electrochemical deposition process originally developed by Yamaura [47] and refined over time by the Hunter group [2, 28, 29]. During deposition in an electrolyte solution, the electrolyte's negatively charged ions are incorporated into the oxidized polymer film as it is deposited, thereby enhancing the conductivity. These films are mechanically robust and feature as-deposited conductivities as high as 10^5 S/m, making them an excellent material from which to slice highly conductive, high aspect ratio PPy microwires. Gold electroplating was also used in order to create gold-backed PPy films with even higher conductivities.

2.3.1 Electrochemical deposition

Electrochemical deposition is conducted using an electrochemical cell which consists of an electrolyte solution and two concentric electrodes, as seen in Figure 2-3. The electrolyte solution contains 0.05 M distilled pyrrole and 0.05 M tetraethylammonium hexafluorophosphate ($TEAPF_6$) in propylene carbonate with 1% (by volume) distilled water. The working electrode and deposition target consists of a glassy carbon crucible 75 mm in diameter and 100 mm in height oriented vertically and submerged approximately 75 mm in the solution. A concentric copper sheet is used as the counter electrode.

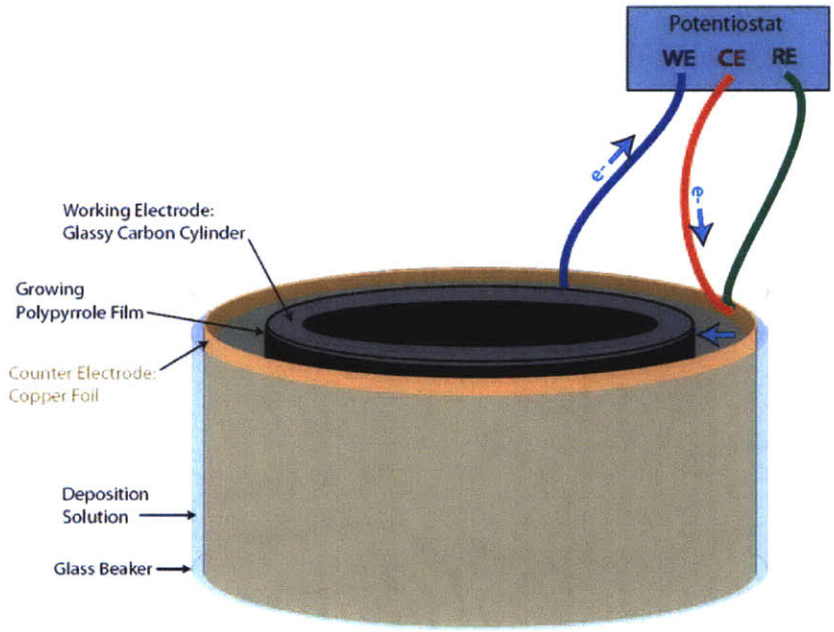

Figure 2-3: A schematic of the electrochemical cell used for polymer deposition. The glassy carbon working electrode and the copper foil counter electrode are placed concentrically in the electrolyte bath. Pyrrole oxidation occurs at the working electrode and results in polymerization and deposition. (Taken from [35])

Before the deposition, the solution is saturated with nitrogen by bubbling nitrogen gas through it while stirring the components. This is done to prevent the premature oxidation of pyrrole. The working and counter electrodes are connected to a potentiostat (Princeton VMP2) with the reference electrode connected to the counter

electrode. In order to better control the rate of polymerization, the electrochemical cell is placed within a temperature chamber (Cincinatti Sub-Zero) and chilled to -40°C prior to applying current to the cell. The deposition is run galvanostatically using a current density of 1 A/m^2 for 10 hours and is controlled using EC-Lab software (Bio-Logic Science Instruments). The resulting films have been optimized for mechanical robustness and are typically about 20 μm thick.

2.3.2 Gold electroplating

The gold layer described in Section 2.2, was incorporated onto the polymer film using an electroplating process. Gold was chosen for its nonreactive nature, high conductivity, and its ability to be electroplated evenly at small thicknesses. It was found to adhere strongly to the electrochemically deposited PPy and did not appear to interfere with the polymer deposition process. The gold layer also reduces the amount of force required to peel the polymer off the substrate, improving the quality of the microwires and increasing yield.

Gold electroplating is conducted before the polymer is electrochemically deposited. The geometry of the electrochemical cell is the same for both processes. Again, the glassy carbon crucible acts as the working electrode and deposition target, and a concentric 316L stainless steel foil is used as the counter electrode. A ready-made neutral non-cyanide gold plating solution (Technic, Inc. Techni Gold 25 ES RTU) is used. The deposition is run galvanostatically with the crucible acting as the working electrode, but in this instance negative with respect to the stainless steel counter electrode. A constant current density of 10.75 A/m^2 is used and results in a calculated deposition rate of 3.79×10^{-10} m/s [14]. The deposition is run for 5 minutes and results in a layer of gold approximately 114 nm thick. After the deposition, the crucible is rinsed by dipping it in distilled water and is allowed to air dry for 15-30 minutes. It is then used for polymer deposition as described in Section 2.3.1, taking care not to rub off the gold layer. Figure 2-4 shows a crucible that has been electroplated with gold and gold backed PPy ribbons partially removed from a crucible.

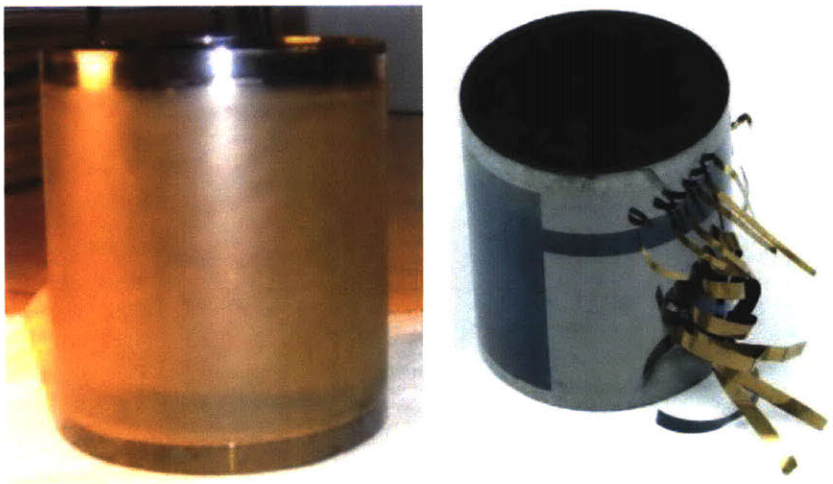

Figure 2-4: (*Left*) Glassy carbon crucible electroplated with gold. (*Right*) Gold-backed PPy ribbons partially removed from crucible. (Taken from [14])

Chapter 3

Conducting Polymer Microwires

Conducting polymer microwires, or fibers, provide good mechanical compliance and high electrical conductivity in a compact form, and are of great interest to the research community. The unique properties of these materials make them useful for a variety of applications ranging from smart textiles to neural recording. Wires with micro- and nano-scale cross-sectional areas have been produced using various fabrication processes and types of conducting polymers. The following sections provide an overview of applications for conducting polymer microwires and descriptions of commonly used fabrication techniques.

3.1 Applications

The intrinsic compliance of conducting polymer microwires has made them ideal candidates for a variety of applications including smart textiles, neural recording, and flexible polymer-based electronics. Their sensitivity to chemical and mechanical stimuli has led to their application in a variety of sensors [26, 31, 39].

3.1.1 Smart textiles

The ubiquity of clothing in human culture coupled with the wide variety of fiber materials and manufacturing techniques makes textiles a logical platform for incorporating

sensing, information processing and actuation. Smart clothing has traditionally been developed by overlaying conventional "hard" electronics onto a textile substrate, resulting in bulkiness and poor wearability. In contrast, nanotechnology offers a means for seamlessly integrating with the textile at various production stages: the fiber spinning, yarn/fabric formation or finishing stage [13]. Textile nanotechnologies have generated significant interest due to their ability to advance functionality while maintaining the look and feel of the fabric. With demand growing in industries ranging from military and security to healthcare and fitness, the market for these technologies is expected to reach $115 billion by 2012 [1].

The conducting polymers polyaniline (PAni) and PPy appear to be the most promising materials for creating functional electronically conducting fibers [23]. Santa Fe Science and Technology has successfully processed PAni using a continuous wet spinning process to produce a textile fiber (Panion^{TM}) which can be manufactured into yarns and a range of fabric structures [6]. The Hunter group has also created PAni fibers via electrospinning [37]. The integration of PPy with textiles has mostly been done by coating fabrics, usually nylon and Lycra, with the polymer using an in situ chemical deposition process [13].

In order to exploit changes in conductivity in response to external deformation, PPy-coated fabrics have been used as flexible strain gauges by the Hunter Group and others, with gauge factors of 6 to 12 being reported [29, 40]. These sensors have been used to develop a device that monitors the wearer's knee joint motion and can be used for rehabilitation following an injury, as shown in Figure 3-1 [31]. PPy-coated polyurethane foams have also been used to monitor breathing and movement of the upper and lower limbs [13]. The two main problems typically affecting PPy-coated fabric sensors are strong variation with time of their resistance, and slow response time following a mechanical stimulus [7]. When properly configured within an electrochemical cell, PPy fabrics may also be used as actuators. Possible applications include human strength augmentation and joint rehabilitation.

Conducting polymers have also been integrated with textiles as chemical detectors because of their high sensitivity to chemical warfare agents [39]. One approach

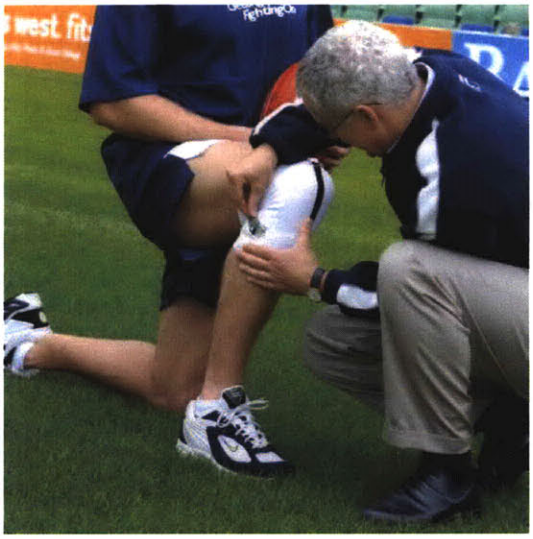

Figure 3-1: The Intelligent Knee Sleeve uses PPy-coated fabric as a strain gauge to monitor the wearer's knee joint motion. Image by CSIRO Textile and Fiber Technology (Taken from [13])

for developing these sensors involves the detection of changes in the resistance of a PPy micro or nanowire caused by a change in its oxidation state in the presence of a chemical contaminant [26]. Another promising approach exploits changes in the refractive index and optical-absorption spectrum of a film following a chemical interaction. These reactions can be detected by coating an optical fiber with a thin film of PAni or PPy, and measuring changes in the optical fiber throughput.

3.1.2 Neural recording

The recording of neuronal activities in the cerebral cortex has contributed to the identification of several brain functions such as reasoning, planning, motor learning, speech, recognition, and auditory and visual processing, among others [5]. Cortical recording is typically conducted using a tightly packed array of sharp microelectrodes which is inserted into the relevant part of the brain [15]. Intravascular neural recording, developed by Hunter Group collaborator Rodolfo Llinas, is a less invasive alternative to traditional techniques which involves placing metal nanowire electrodes in capillaries adjacent to the target neurons. Experiments have demonstrated that the

electric potential of a neuron near a capillary can be sensed by an electrode within the capillary due to the relatively small electrical impedance of the blood-brain barrier [25].

Platinum, iridium and tungsten are commonly used as electrode materials because of their high electrical conductivity, low reactivity, and high resistance to corrosion. The significant mismatch in the compliances of "soft" brain tissue and "stiff" metal electrodes often causes shear-induced inflammation and scarring, limiting long term recording by electrically and mechanically isolating the target neurons [9]. Reductions in the size of the microelectrodes and the development of "flexible" arrays have alleviated but not eliminated the risk of tissue damage. The compliance mismatch has also made difficult the implementation of the intravascular technique. The high bending stiffness of the platinum nanowires causes them to puncture the vessels while navigating through the curving paths of the capillary bed. This compliance mismatch may be resolved by replacing metals with PPy microwires.

Neural recording with PPy microwires has been demonstrated using both the intravascular technique and traditional invasive cortical recording. Bryan Ruddy of the Hunter Group produced PPy microwire electrodes which were used by the Llinas group for high-fidelity neural recording through a blood vessel wall in a frog [37]. Figure 3-2 shows the experimental setup for intravascular recording in a frog and electrode signals recorded after nerve stimulation. Woong Jin Bae of the Bizzi Group at MIT, in collaboration with the Hunter Group, fabricated PPy microwire electrodes and inserted them in a rodent brain to record cortical neural activity [3]. Figure 3-3 shows the electrode used for cortical recording as well as the recorded action potentials.

3.1.3 Polymer-based electronics

Conducting polymers figure prominently among the organic materials commonly used to develop flexible electronic components and devices such as thin film field-effect transistors, LEDs, photodiodes, batteries, and displays, among others [7]. Nathan Wiedenman of the Hunter Group developed all-polymer electrical components using

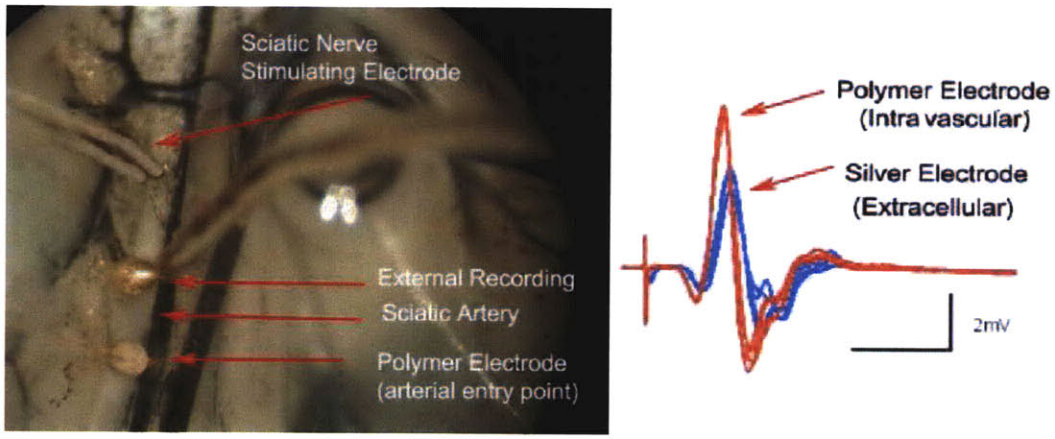

Figure 3-2: (*Left*) Experimental setup for intravascular recording of sciatic nerve signals in a frog using a conducting polymer electrode. (*Right*) Electrode signals recorded from the frog sciatic nerve after stimulation. Images courtesy of Rodolfo Llinas. (Taken from [37])

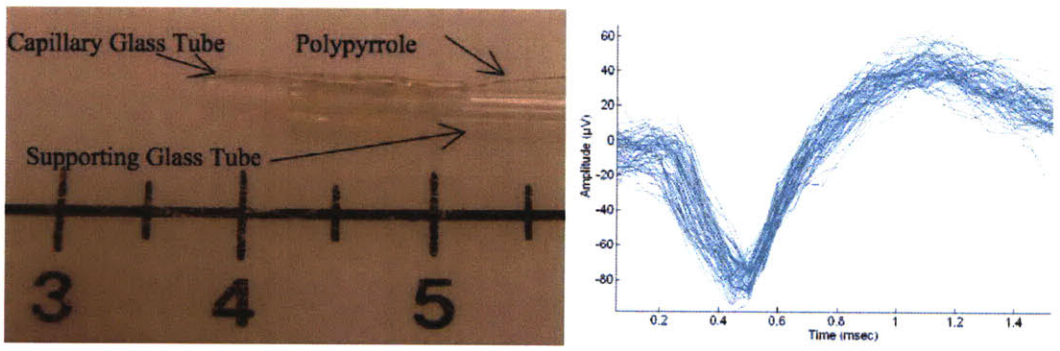

Figure 3-3: (*Left*) The recording end of a PPy microwire electrode. (*Right*) Overlaid action potentials from raw data recorded in a rat brain. (Taken from [3])

co-fabrication techniques and proposed their integration into conducting polymer feedback devices [46]. The intrinsic compliance of conducting polymer microwires makes them ideal for electrically interconnecting such devices. They may also be used as antennas to provide wireless interconnectivity between separate devices.

3.2 Fabrication Techniques

Various techniques have been developed for fabricating conducting polymer microwires and nanowires. These techniques can generally be classified into three separate categories: template-based deposition, template-free and post-fabrication size reduction techniques. This chapter provides a brief description and discussion of these methods.

3.2.1 Template-based deposition techniques

Templated deposition techniques involve the deposition of conducting polymer onto a non-conducting-polymer substrate, the shape of which tightly controls the size and morphology of the resulting polymer microwires. One method calls for polymerizing PPy or PAni onto carbon nanotubes and organic polymer nanofibers [27, 48]. The use of these nanofiber templates limits the amount of conducting polymer on the finished wire and often results in rough surface morphologies and nonmetallic conductivities on the order of a few Siemens per meter. Another method involves polymerizing within the pores of microporous substrates, such as microporous alumina, and track-etched polyester and polycarbonate membranes [8, 30]. The range of aspect ratios provided by microporous substrates is limited and the resulting microwires are usually only a few micrometers in length.

In general, the nonmetallic conductivity and short length of microwires produced using these techniques makes them unsuitable for neural recording, smart textiles and other applications that require good electrical conduction over lengths of many millimeters. Microwires produced using these techniques can be seen in Figure 3-4.

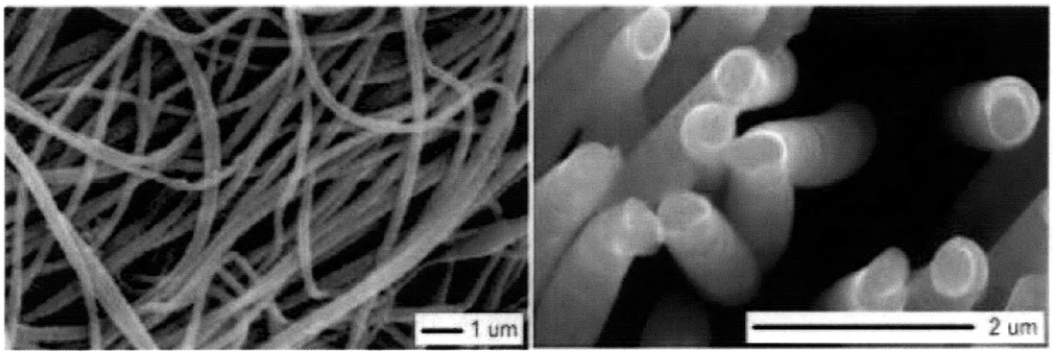

Figure 3-4: (*Left*) Polyacrylonitrile microwires coated with PPy (Taken from [27]) (*Right*) PPy microwires synthesized within the pores of a track-etched polycarbonate membrane (Taken from [30])

3.2.2 Template-free techniques

Techniques that do not require the use of templates have also been used to produce conducting polymer microwires. Electrospinning is one such technique that is increasingly being used for the production of PPy and PAni microwires [11, 27, 37]. This technique uses high electric fields (tens of kVs) to stretch a jet of polymer dissolved in solvent. As it travels through the electric field, the jet is further elongated by a whipping instability, and is finally deposited on the grounded collector in the form of micro or nanowires. Electrospun microwires can be meters in length and can be fabricated coaxially with an insulator coating [37]. Unfortunately, reported wire conductivities are poor, on the order of a few siemens per meter [11, 37]. Figure 3-5 shows PPy and PAni electrospun microwires.

Wet spinning has also been used to produce PPy and PAni microwires [6, 16]. This technique involves pushing polymer dissolved in solvent through fine holes in a spinneret and into a coagulation bath, where it solidifies into a fiber. The fibers can then be heated and stretched using two godets, or rollers, rotating at different speeds. Stretching the fibers both decreases their final cross-sectional area and increases their conductivity by increasing polymer chain alignment. Wet spun PAni fibers (Panion^{TM}) can be many meters long and with diameters of about 100 μm, elastic modulus of 3 to 6 GPa, ultimate strength of 100 to 300 MPa, final strains of 5 to 60%, and conductivities of 7,200 to 72,500 S/m [6]. Previous work has shown

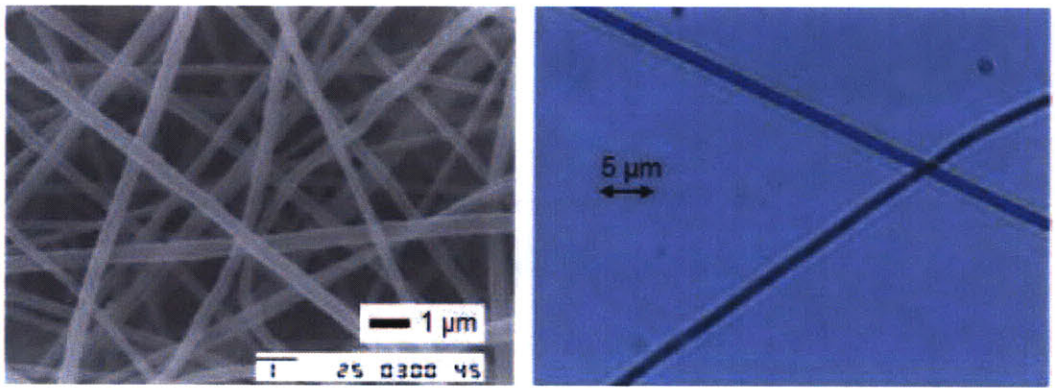

Figure 3-5: (*Left*) Electrospun PPy/PEO microwires. PPy content is 71.5 wt%. (Taken from [11]) (*Right*) Coaxially electrospun PAni-CSA/PEO microwires produced by the Hunter Group. (Taken from [37])

that the strength and stiffness of wet spun PAni fibers can be improved through the addition of single-walled carbon nanotubes [43]. Un-stretched wet spun PPy wires have been produced with diameters of about 150 μm, modulus of 1.5 GPa, ultimate strength of 25 MPa, final strain of 2%, and conductivity of 300 S/m [16]. Figure 3-6 shows PPy and PAni wet spun microwires.

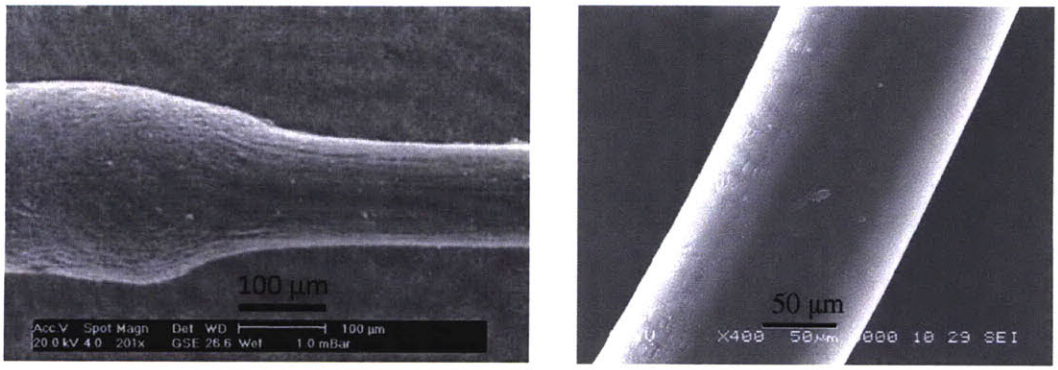

Figure 3-6: (*Left*) Wet spun PAni microwire (Panion^{TM}) during stretch alignment. (Taken from [6]) (*Right*) Un-stretched wet spun PPy microwire. (Taken from [16])

3.2.3 Post-processing techniques

Conducting Polymer microwires may be produced by additional processing of the bulk material after polymer synthesis. Meso-scale fibers can be thermally drawn to

produce fine microwires. Microwires can also be sliced from thin polymer films.

A group at MIT has developed a thermal drawing technique for fabricating long, non-conducting polymer fibers [4]. It involves preparing a tubular preform (12.5 mm diameter) composed of a conductor, amorphous semiconductors and polymeric insulators which is subsequently heated and drawn into a fiber (500 μm diameter) that preserves the initial geometry. Conducting polymer microwires could be produced by using a preform of melt-processable conducting polymer, insulation and easily removed filler, and performing multiple stages of thermal drawing to achieve the required size reduction [37]. There are a few readily melt-processed conducting polymers, but they tend to have lower conductivities and very poor actuation performance [45].

The Hunter Group has produced conducting polymer microwires by slicing previously synthesized polymer films using two methods. The first approach involves producing a PPy film using the deposition process described in Section 2.3, and encapsulating it in a block of ice [37]. The block is then attached to a cryo-microtome sample holder and sliced into 20 μm sections, producing 20 mm long microwires with a 20 μm $\times$ 20 μm square cross-section, as shown in Figure 3-7. The geometry of this technique dictates that the sliced wire can only be as long as the cutting blade, thus limiting the maximum wire length to 20 to 30 mm.

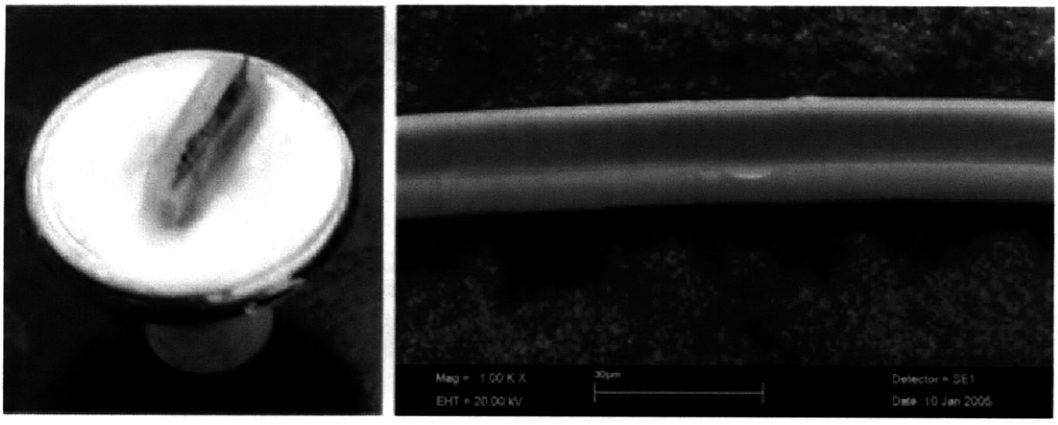

Figure 3-7: (*Left*) Mounted ice block with embedded PPy film. (*Right*) PPy microwire sliced from a film using a cryo-microtome. The scale bar equals 30 μm. (Taken from [37])

The second approach involves mounting a glassy carbon cylindrical crucible, coated with the deposited PPy film, onto the main rotary axis of a turning center (Mazak Super Quick Turn 15MS) [14]. A razor blade attached to a custom-built tool slices a spiral along the film to produce microwires with varying thicknesses of a few tens of micrometers and lengths of a few millimeters, as shown in Figure 3-8. It is believed that the incorporation of additional hardware and further automation of the process could lead to the consistent production of fine continuous microwires. This thesis describes work done towards this goal.

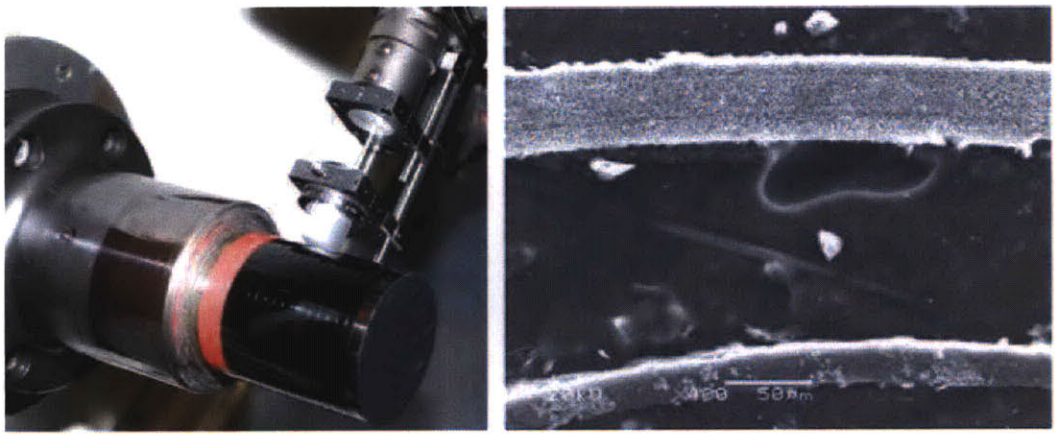

Figure 3-8: (*Left*) PPy film on a glassy carbon crucible being sliced in the Mazak turning center. (*Right*) Gold-backed PPy microwires sliced to widths of about 50 μm. The scale bar equals 50 μm. Images by Nathan Wiedenman. (Taken from [14])

Chapter 4

The Microwire Slicing Instrument

The Hunter Group's research on conducting polymer actuators and neural electrodes has led to the production of conducting polymer microwires using various fabrication techniques. As described in Section 3.2.3, microwires have been produced by cutting electrodeposited PPy films using both a cryo-microtome and a Mazak turning center, but their lengths have been limited to a few tens of millimeters [14, 37]. Coaxially electrospun PAni-CSA/PEO microwires have also been produced, but their conductivities were poor compared to those made from PPy films [37].

This work builds upon these previous efforts and involves the development of an instrument capable of producing conducting polymer microwires with both high conductivities and significantly longer lengths. In order to ensure high conductivity and mechanical robustness, the wires were sliced from thin PPy films electrodeposited onto a glassy carbon crucible. The instrument slices the film by running a sharp blade over the crucible in a helical pattern. The blade is simultaneously slid along its length such that a fresh cutting edge is continuously presented at the point of contact with the crucible. This instrument has enabled the production of PPy microwires with widths as small as a few microns and lengths ranging from tens of millimeters to meters. It may also be used to slice microwires from films made of other types of conducting polymers. The design of the wire cutting instrument and the automation of the cutting process is described in the following sections. Work done towards the development of a wire uptake system is also presented.

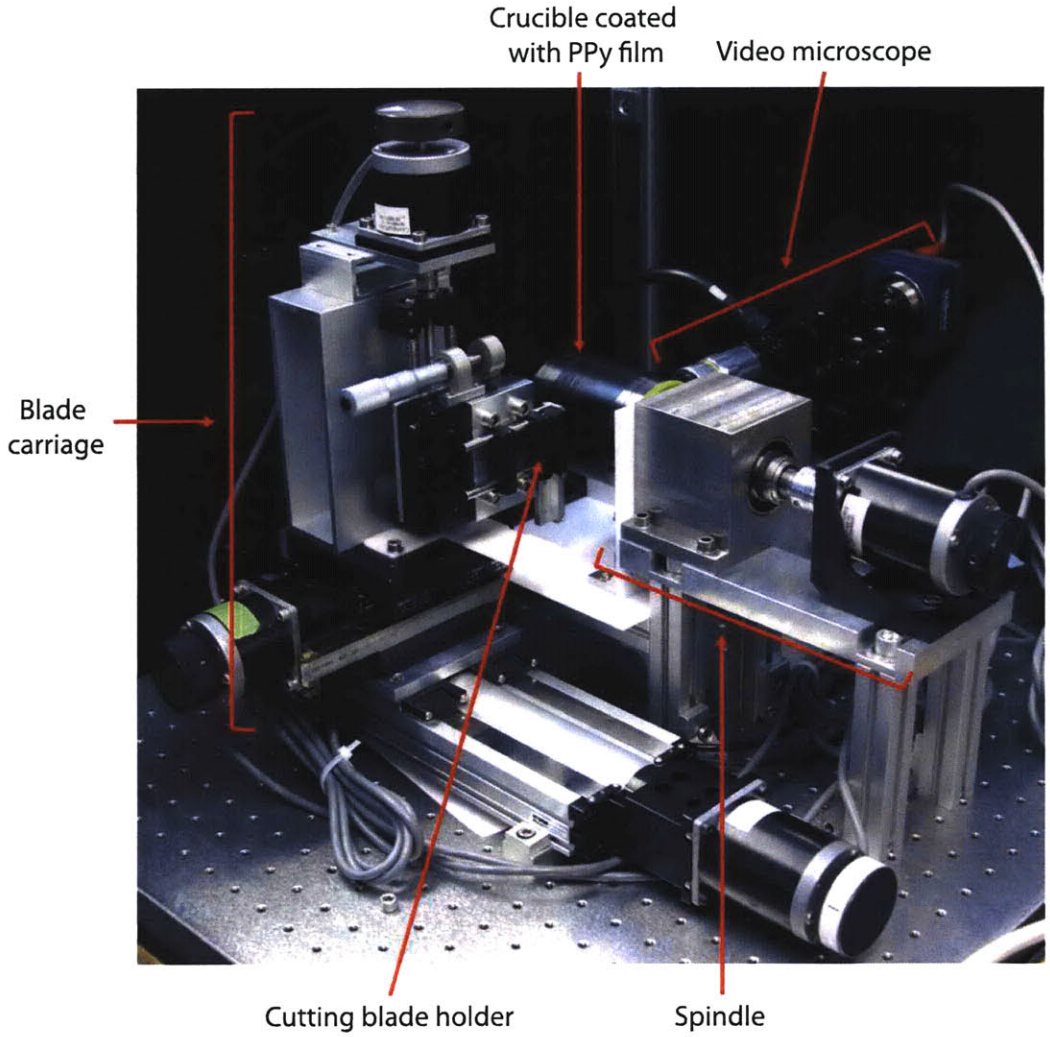

Figure 4-1: The microwire slicing instrument.

4.1 Instrument Design

The main functional requirement for the microwire slicing instrument, depicted in Figure 4-1, was to accurately produce the complex motions involved in the combined helical and blade sliding cutting operation. The instrument would be controlled using a computer, and allow for the visual inspection of the freshly cut microwires. It was also desired to have a modular design capable of accommodating glassy carbon crucibles of various sizes.

The general layout of the instrument is similar to that of a typical turning center or lathe. In order to generate the required cutting path, the instrument features three linear axes labeled Z, X and V, and one rotary axis labeled C. As shown in Figure 4-2, the Z-axis runs parallel to the length of the crucible, and the X and V axes run perpendicular to the crucible in the horizontal and vertical direction, respectively. The instrument can be divided into three modules: the spindle, the cutting blade carriage, and the video microscope.

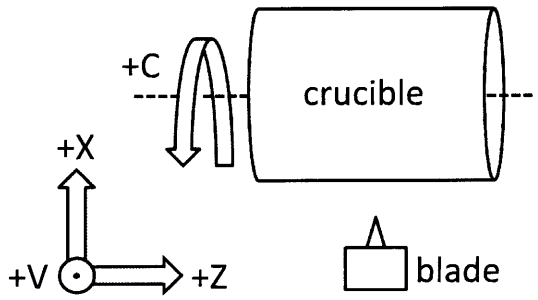

Figure 4-2: Schematic of the wire cutting instrument's four axes. The blade is moved relative to the crucible along the X, Z, and V axes, and the crucible is rotated about the C-axis.

4.1.1 Spindle

The spindle provides a secure attachment for the glassy carbon crucible and rotates it about the C-axis. Its main component is a custom-built steel shaft and bearing block assembly driven by a stepper motor (Parker ZETA). The crucible, coated with an electrodeposited PPy film, is loaded horizontally onto a machined plastic (oil-filled

cast nylon) holder that fits onto the shaft, as depicted in Figure 4-3. The cylindrical holder is attached to the shaft using set screws, and its outer surface fits snug with the inner surface of the crucible. Two disc magnets, one on the end of the crucible and another at the end of the shaft, secure the crucible against the holder and prevent it from turning during cutting.

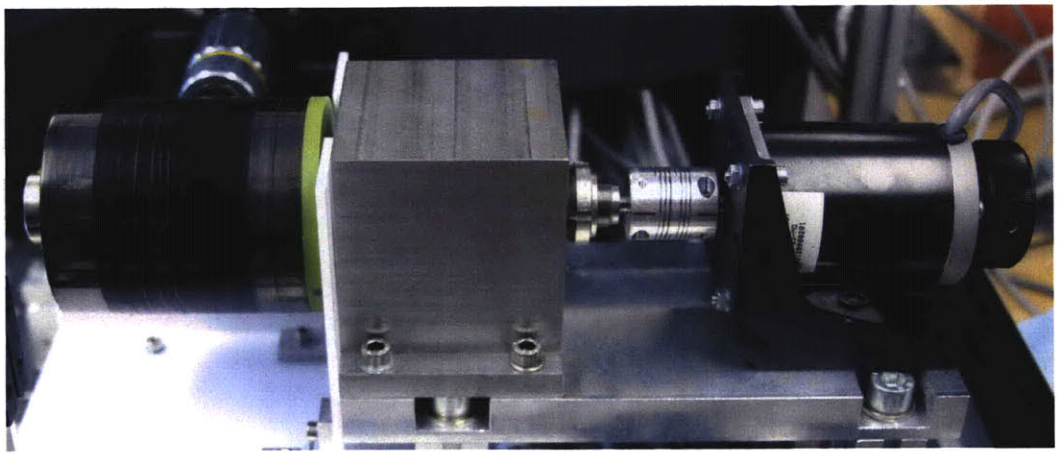

Figure 4-3: A glassy carbon crucible loaded on the spindle.

In order to minimize axial and lateral play during rotation, the spindle assembly was carefully designed to ensure that the shaft was properly constrained. The shaft is supported by two ABEC-3 angular contact bearings (SKF 7204 BEP) housed in a bearing block, and positioned three shaft diameters apart in a back-to-back configuration[1]. The bearings are secured against a shoulder on the left end of the shaft, a shoulder inside the bearing block, and a locknut (Whittet-Higgins) that screws onto the right end of the shaft, as shown in Figure 4-4. A preload was applied by tightening the locknut until there was no play in the shaft. Disc springs were placed between the locknut and the bearing in order to better control the applied preload and reduce vibrations. A flexible helical coupling (Ruland) is used to attach the shaft to the stepper motor. Detailed drawings of the shaft and the bearing block can be found in Appendix A.

[1]Information on the design of bearing assemblies can be found in [20], [32], and [41].

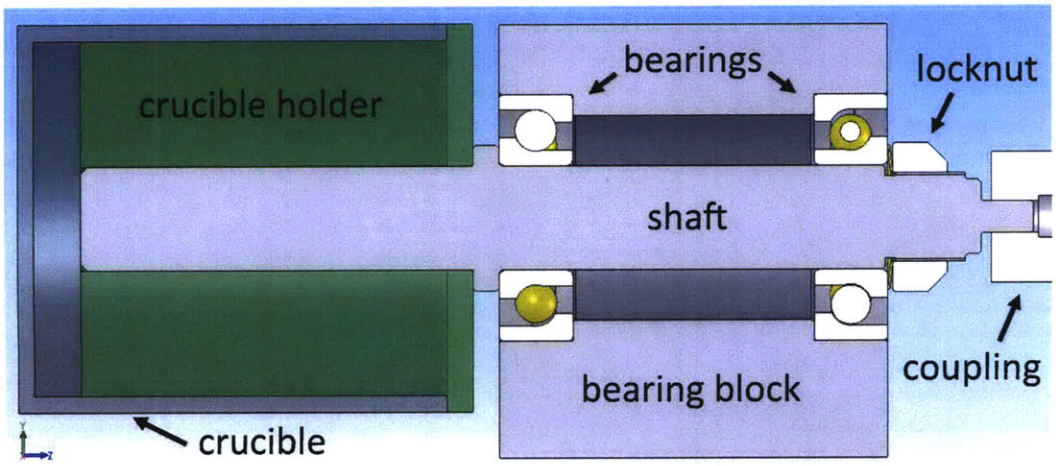

Figure 4-4: Cutaway schematic view of the spindle assembly. For scale, the shaft has a main diameter of 20 mm.

4.1.2 Blade carriage

The blade carriage provides a secure attachment for the cutting blade and moves it along the X, Z and V axes. Initially, microtome blades 76 mm long and 8 mm wide were used to slice the PPy film, but they tended to leave deep scratches on the crucible surface. Gillette razor blades 36 mm long and 5.5 mm wide were found to cut well while minimizing damage to the crucible. A machined aluminum holder, shown in Figure 4-5, is used to attach the desired cutting blade to the overall carriage. The length of the blade is oriented vertically because the cutting angle of the helical motion required to slice wires less than 3 mm wide is approximately 90°. The equation for the cutting angle is derived in Section 4.2.1.

Measurements carried out early in the design process revealed that the crucible diameter changes by up to 1 mm from one end of the crucible to the other. In order to accommodate these changes in the crucible diameter, the blade needs to be preloaded against the crucible surface during cutting. Initially, the blade holder was attached to a spring-loaded, sliding bearing linear stage (Linos Microbench), as depicted in Figure 4-6. Cutting tests showed that this configuration was applying an excessive (>10 N) and variable normal force on the blade. This was evidenced by significant blade wear and varying degrees of ruffling and tearing along the length of the cut

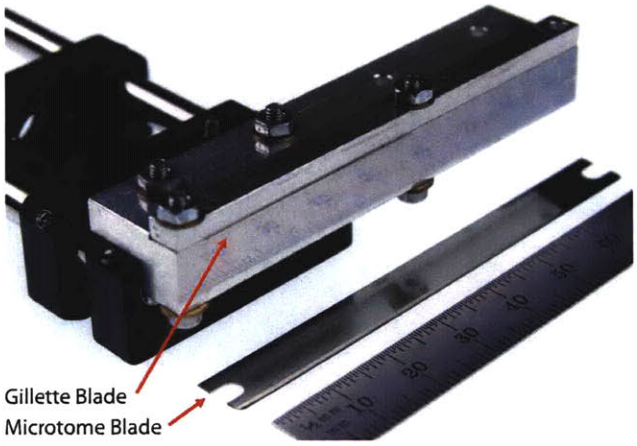

Figure 4-5: A Gillette blade is shown clamped onto the blade holder. Alternatively, a microtome blade may be clamped to the bottom surface of the holder.

microwires. In order to reduce variations in the force and apply a lighter preload, the sliding bearing stage was replaced by a spring-loaded, ball bearing linear stage (Newport M-423). The new stage allows for significantly smoother movement, and can accommodate a number of softer springs which provide preloads in the range of 0.5 N to 8 N. The blade holder and ball bearing stage are collectively referred to as the blade holder assembly.

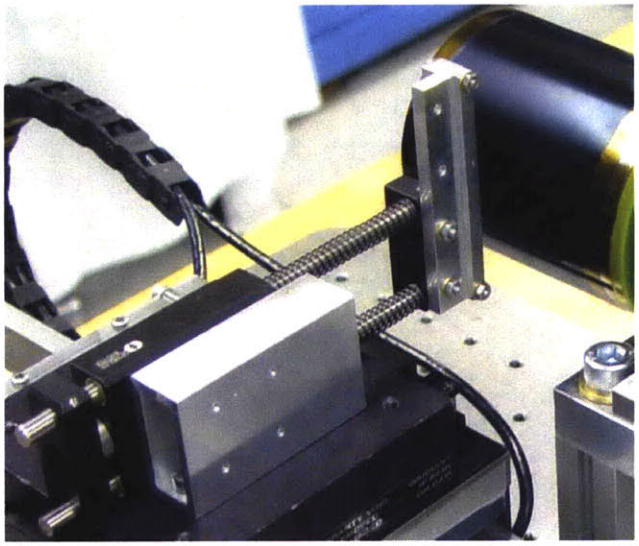

Figure 4-6: An early design which preloaded the blade against the crucible surface using a spring-loaded, sliding bearing stage.

The blade holder assembly is mounted onto a vertically oriented, 30 mm travel linear stage. This stage provides motion along the V-axis using a fine-pitch leadscrew and is spring-loaded to prevent backlash. Motion along the X and Z axes is provided by linear stages (NEAT and Parker) with travels of 50 mm and 150 mm, respectively. As shown in Figure 4-7, the three stages are mounted onto each other and are actuated by stepper motors (Parker ZETA).

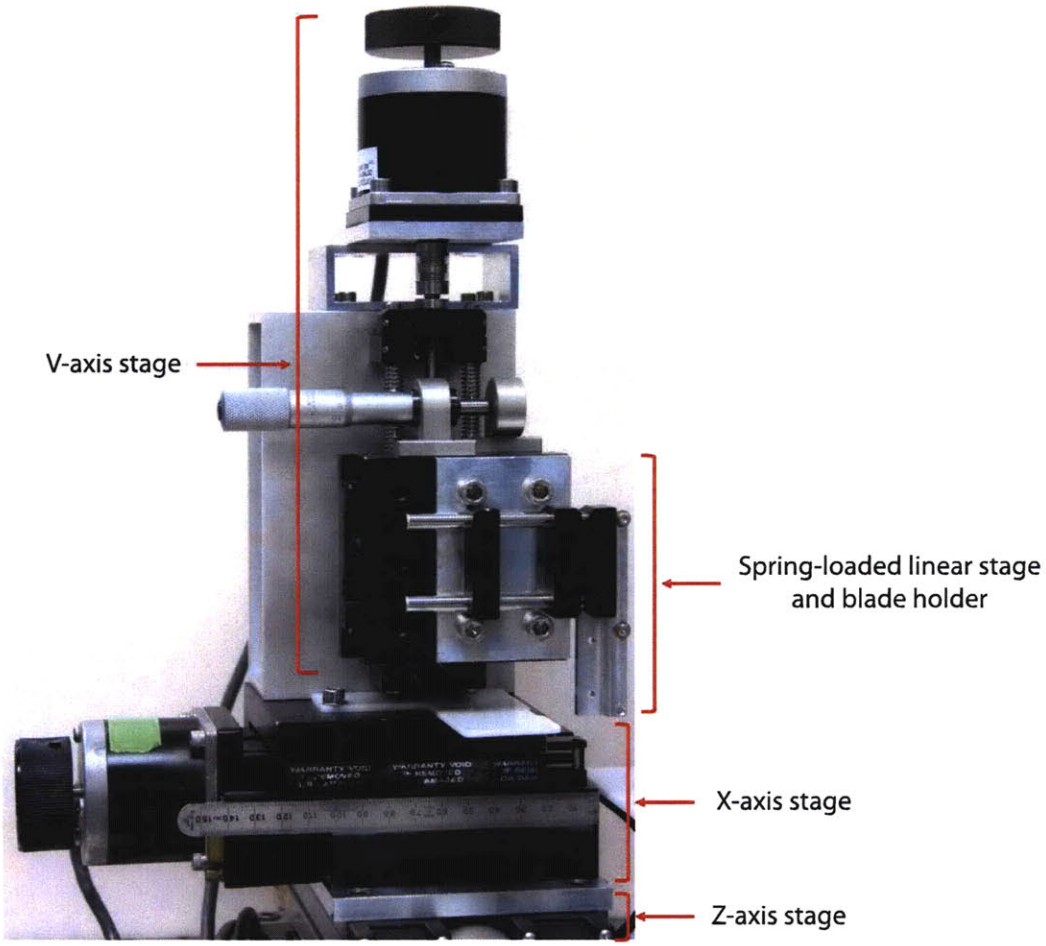

Figure 4-7: The fully-assembled blade carriage. It provides a secure attachment for the cutting blade and moves it along the X, Z and V axes.

4.1.3 Video microscope

The video microscope provides a magnified image of the crucible surface and allows the operator to visually inspect the freshly sliced microwires. It is composed of an infinity-corrected long working distance microscope objective (Mitutoyo), a 200 mm focal length tube lens (Infinity InfiniTube^{TM}Standard), and a CCD camera (Unibrain Fire-i 701c), as shown in Figure 4-8. A fiber optic illuminator (Schott KL 1500) is attached to the tube lens assembly in order to provide in-line illumination. This flexible architecture allows for the attachment of objectives with 2× to 100× magnification in order to observe wires of different sizes. The device is mounted on two manual linear stages (Newport M-TSX-1D) which allow for fine adjustments along the X and Z axes. The camera is connected to a desktop computer and LabVIEW software is used to view a color image on the monitor.

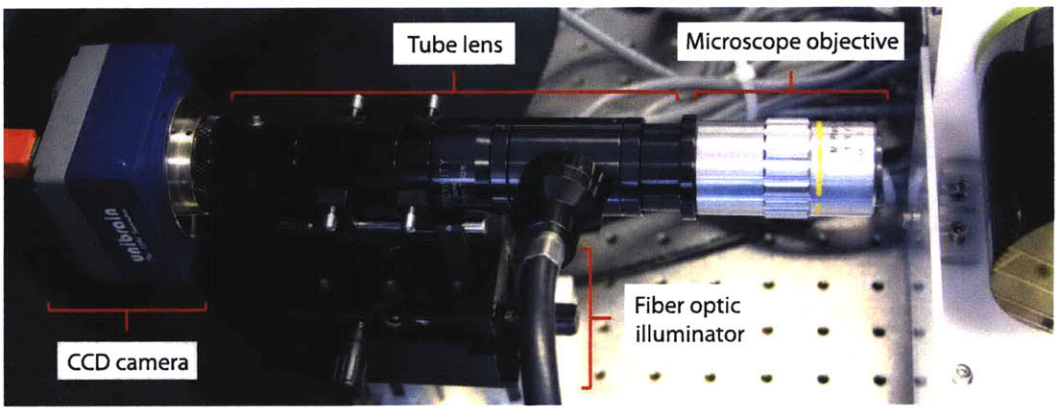

Figure 4-8: The video microscope used to view the PPy microwires after cutting.

4.2 Process Automation

The task of automating the wire slicing process began with the development of a series of equations that described the relevant geometry of the desired helical cutting path. Motion control software and hardware where then used to implement these equations in order to precisely coordinate the motions of the wire instrument's axes.

4.2.1 Continuous wire cutting geometry

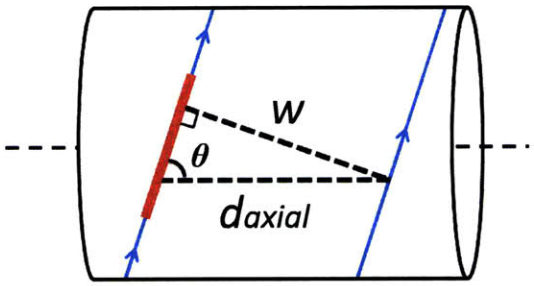

Figure 4-9: A continuous wire is produced by sliding a blade (red) along a helical path (blue) on the surface of the cylindrical crucible. This schematic shows the relationship between the axial displacement d_{axial}, the ribbon width w, and the cutting angle θ. (Figure not to scale)

A continuous wire of length L can be sliced from a PPy film deposited on a cylindrical crucible by cutting a helical path along its surface as shown in Figure 4-9. Considering one revolution, the axial displacement d_{axial} can be related to the wire width w by

$$sin\,\theta = \frac{w}{d_{axial}}, \tag{4.1}$$

where θ is the cutting angle with respect to the horizontal axis. The axial displacement and the tangential displacement d_{tan} along the surface of the crucible after one revolution are related by

$$tan\,\theta = \frac{d_{tan}}{d_{axial}} = \frac{\pi D}{d_{axial}}, \tag{4.2}$$

where D is the diameter of the crucible. Combining these equations, we find that the cutting angle, as a function of the wire width, is given by,

$$\theta = arccos\left(\frac{w}{\pi D}\right). \tag{4.3}$$

Therefore, the ratio between the tangential and axial displacements, as a function of the desired ribbon width, is given by the equation

$$\frac{d_{tan}}{d_{axial}} = \frac{\pi D}{w}\sqrt{1-\left(\frac{w}{\pi D}\right)^2}. \tag{4.4}$$

Finally, the length L of the ribbon, as a function of the desired ribbon width and the total axial displacement, is given by

$$\begin{aligned} L &= \sqrt{(N \cdot \pi D)^2 + {d_{axial}}^2} = \sqrt{\left(\frac{d_{axial}\, sin\,\theta}{w} \cdot \pi D\right)^2 + {d_{axial}}^2} \\ &= \sqrt{\left(\frac{d_{axial}}{w}\sqrt{1 - \left(\frac{w}{\pi D}\right)^2} \cdot \pi D\right)^2 + {d_{axial}}^2}, \end{aligned} \tag{4.5}$$

where N is the number of revolutions as a function of the desired width and the total axial displacement.

4.2.2 Motion control hardware and software

The microwire slicing instrument is integrated with motion control hardware and software in order to automate the wire slicing process. A basic block diagram of the instrument is shown in Figure 4-10. The stepper motors are each commanded by separate stepper drives (Parker ZETA4), and the X and Z axes are fitted with linear optical encoders (Renishaw) which allow for closed loop position control. The stepper drives and encoders are connected to a connector box (NI UMI-7764) powered by a 5 V DC power supply (HP E3610A). The connector box interfaces with a 4-axis motion controller (NI PCI-7354) connected to a desktop computer running NI LabVIEW software.

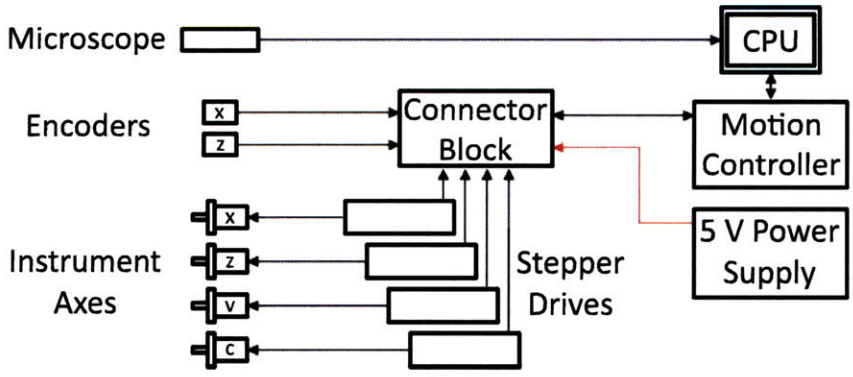

Figure 4-10: A block diagram of the wire cutting instrument.

It was decided that the automated helical cutting process would require the user

to specify three parameters: the desired wire width (in mm), the rotational speed of the C-axis (in rev/s), and the desired displacement along the Z-axis (in mm). The Z-axis displacement is used instead of the wire length because the former allows the operator to better specify the cutting area and avoid crashing the blade carriage into the spindle assembly. In this instrument, the C-axis rotates to provide a tangential displacement of πD mm/rev at the surface of the crucible, and the Z-axis provides an axial displacement with a pitch of 5 mm/rev. Using this information and the specified parameters, we can rewrite Equation 4.4 and define the ratio of C-axis to Z-axis motor revolutions needed to achieve the helical cutting motion. This ratio GR is given by the equation

$$GR = \frac{5}{w}\sqrt{1 - \left(\frac{w}{\pi D}\right)^2}. \tag{4.6}$$

The resulting Z-axis velocity (in mm/s) is given by the equation

$$V_{Z-axis} = \frac{5\omega_c}{GR}, \tag{4.7}$$

where ω_c is the rotational speed of the C-axis (in rev/s).

These equations are implemented in a LabVIEW program used to control the instrument [12]. The program features a graphical user interface, shown in Figure 4-11, which allows the operator to specify the three cutting parameters described above. The displacement and speed of the V-axis, and the speed of the X-axis may also be specified. Once the parameters are entered, the program uses the derived equations to calculate the required axis trajectories, and then uses the motion controller to command the axes. The program first advances the blade along the X-axis to the crucible surface. The C and Z axes then move the blade along the helical trajectory, and the V-axis slides it vertically. If the specified V-axis displacement (it cannot exceed the blade length) is reached, the axis simply reverses its direction. Once the cut is completed, the blade is retracted off the crucible surface.

Two additional LabVIEW programs were written to provide alternative modes of operation. One of these programs allows the operator to move each axis independently. The second program slices the polymer film into rings of a desired width.

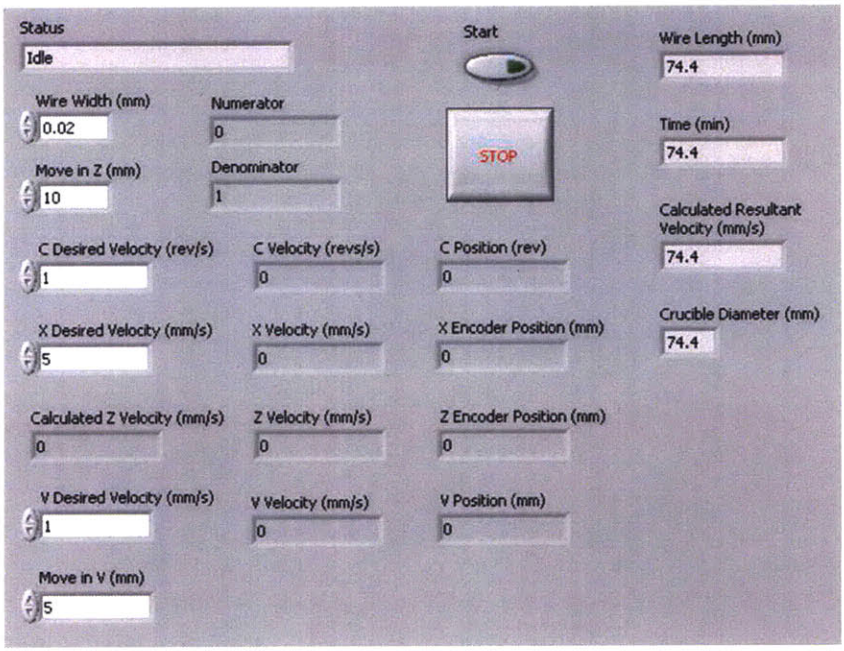

Figure 4-11: The LabVIEW control panel that allows the operator to specify the parameters controlling the helical cutting process.

4.3 Wire Removal and Uptake

After running a sharp blade over the PPy film in a helical pattern, the resulting wire must be removed from the surface of the crucible. Wide PPy wires (width > 0.5 mm) can typically be removed manually after cutting because they adhere to the crucible and are strong enough to resist tearing. Wires with finer widths are more prone to tearing due to defects in the material and irregularities on the crucible surface. They are also more likely to peel off during the cutting operation and may become entangled on the blade. These factors generally prevent the generation of single, continuous wires several meters long. Therefore, the production of long, fine wires requires a wire uptake system capable of peeling the wires off the crucible as they are cut.

4.3.1 Passive wire uptake system

A passive, linear uptake system was implemented and tested as an intermediate step to an active wire spooling system. The passive system consists of a mass attached to the PPy wire via a string and suspended by a pulley, as shown in Figure 4-12. As the crucible turns, the mass descends due to gravity and applies tension on the wire, peeling it off the crucible.

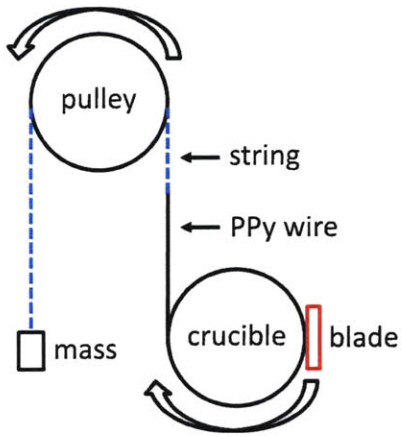

Figure 4-12: Schematic of the passive wire uptake system.

Tests with 20 μm thick gold-backed PPy films demonstrated the successful peeling of 1 mm wide wires using 0.5 N of tension, and 100 μm and 200 μm wide wires using 0.2 N of tension. The finest wire successfully removed using this apparatus had a 100 μm $\times$ 20 μm cross-section and was 1.2 m long (See Figure 5-9). Wires would sometimes fracture during testing because of either excessive or insufficient tensioning. Under-tensioning would cause the wires to break after they failed to peel tangentially off the crucible. The finer wires were more prone to failure by over tensioning because they are typically not as strongly adhered to the crucible surface. These results indicate that precise control of the wire tension is critical to production of long, fine PPy microwires, and underline the need for an active wire uptake system.

4.3.2 Proposed active wire uptake system

The main functional requirement of the active wire uptake system is to spool the PPy microwire while keeping it in constant tension. For a 20 μm $\times$ 20 μm cross-section wire, the tension must not be greater than 30 mN to avoid yielding and breaking the wire. A proposed design of the system, depicted in Figure 4-13, involves two thin, rotating shafts mounted on jewel bearings, and connected by a torsion spring. A small DC motor drives one of the shafts, and the PPy microwire is spooled onto the other. Non-contact optical encoders are mounted on both shafts and measure their angular position. The applied tension is related to the stiffness of the spring and the difference in the shafts' angular position. A control system must be developed to set the angle difference, and thus the tension, using the DC motor.

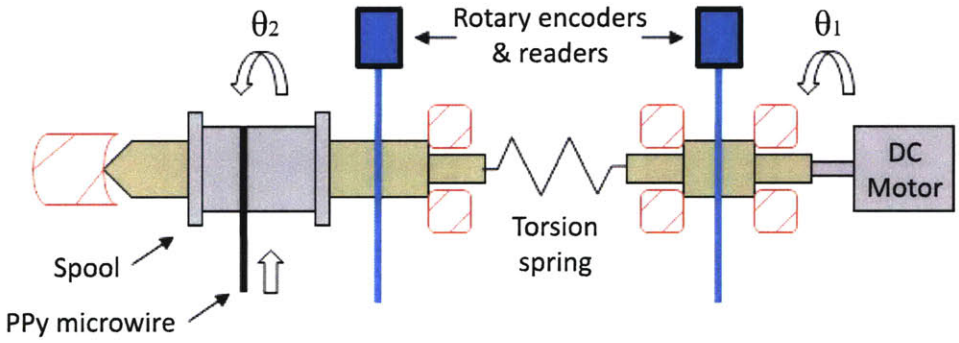

Figure 4-13: Schematic of the proposed active wire uptake system.

Chapter 5

Characterization of the Microwire Slicing Instrument

The operation of the microwire slicing instrument is controlled by user-defined process parameters such as the axis speeds and the blade preload. The effect of these parameters on the helical slicing process must be well understood in order to determine optimal settings for the production of high quality PPy microwires. Extensive testing was performed to characterize the effects of different parameter settings on blade wear and wire morphology. The results of these tests are presented and discussed in the following sections. The current capabilities and limitations of the microwire slicing instrument are also discussed.

5.1 Blade Wear Tests

Continuously sliding a steel Gillette blade over the surface of the glassy carbon crucible results in visible wearing of the cutting edge. This damage prevents the PPy film from being sliced properly and may result in structurally weak microwires with ruffled edges. The level of damage resulting from different parameter settings was characterized in order to determine how to minimize blade wear.

Cutting tests were performed using six different parameter sets which consisted of high and low values of blade preload, C-axis speed, cut length, and V-axis speed, as

Set	Preload (N)	C-axis speed (rev/s)	Cut length (m)	V-axis speed (mm/s)
1	3	0.2	5.84	0
2	3	1.5	5.84	0
3	3	0.2	58.4	0
4	6	0.2	5.84	0
5	3	0.2	5.84	0.5
6	3	0.2	5.84	5

Table 5.1: Sets of cutting parameters used in blade wear tests.

shown in Table 5.1. For simplicity, the four process parameters were varied one at a time and the wire width was kept constant at 20 μm. The values were chosen based on some preliminary testing and the C-axis speeds were chosen to be compatible with the expected operating speed of the proposed wire uptake system. The two cut lengths are equivalent to displacements of 0.5 and 5 mm along the Z-axis, respectively.

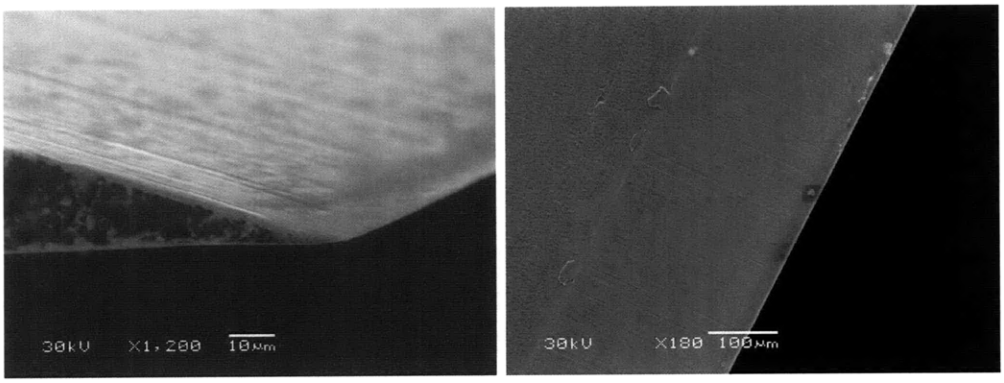

Figure 5-1: SEM images of an unused Gillette blade.

SEM images of an unused control blade and worn test blades are shown in Figures 5-1 and 5-2, respectively. Figure 5-2 shows that a burr forms on the cutting edge as the blade is dragged over the glassy carbon surface. If the cut length is on the order of tens of meters, the burr eventually detaches from the blade and leaves behind a jagged cutting edge, as seen in Figure 5-2(c). A comparison of Figures 5-2(a) and 5-2(b) suggests that there is little variation in burr size (about 16 and 19 μm, respectively) between the tested C-axis speed values (0.2 vs. 1.5 rev/s). As can be expected, Figure 5-2(d) shows that increasing the preload significantly increases the size of the burr to about 27 μm. Figures 5-2(e) and 5-2(f) demonstrate that moving the blade along the

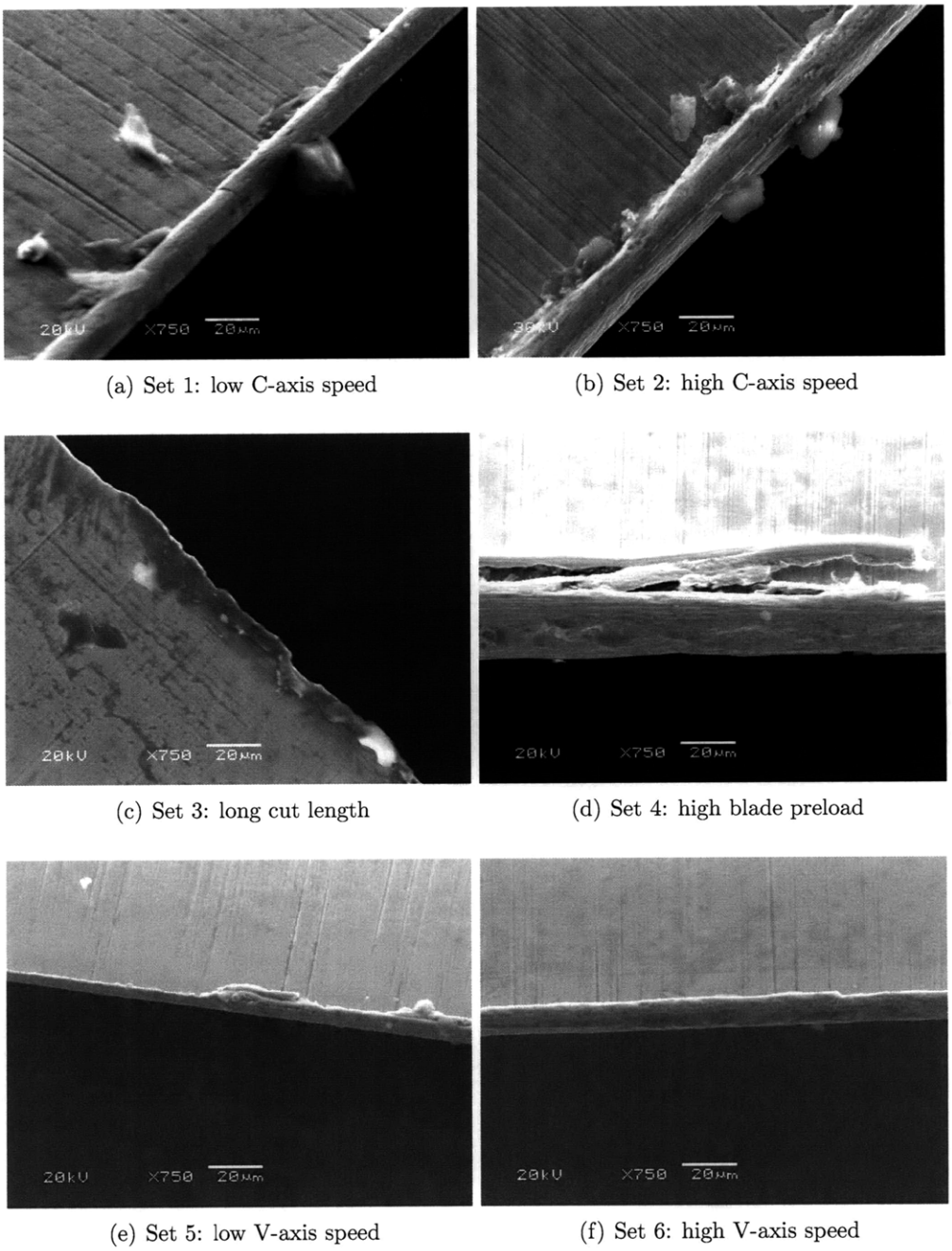

(a) Set 1: low C-axis speed

(b) Set 2: high C-axis speed

(c) Set 3: long cut length

(d) Set 4: high blade preload

(e) Set 5: low V-axis speed

(f) Set 6: high V-axis speed

Figure 5-2: SEM images of worn Gillette blades subjected to different sets of cutting parameters. Images (a), (d), (e), and (f) were taken by Lauren Montemayor.

V-axis results in smaller burrs about 7 and 11 μm in size, respectively.

These results indicate that the cutting blade wears significantly during the slicing process and can develop burrs almost as large as the microwires themselves. The damage can be minimized by applying a low preload force ($\leq$3 N) and limiting the length of the cut. Sliding the blade along the V-axis uses a larger part of the cutting edge and significantly reduces wear at low speeds ($\leq$0.5 mm/s).

5.2 Microwire Slicing Tests

Slicing tests were performed to determine the effect of different cutting parameter settings on the quality of PPy microwires sliced from both gold-backed (PPy/Au) and neat PPy films 20 μm thick. The desired microwire width was set to 20 μm in order to produce wires with square cross-sections. Six different settings involving high and low values of C- and V-axis speeds were used, as shown in Table 5.2. The blade preload and the cut length were set to 3 N and 5.84 m, respectively, in order to minimize blade wear. The freshly sliced films were imaged at 10$\times$ magnification using the video microscope. Short lengths of wire were then carefully removed by hand from near the beginning and the end of the cut, and imaged using a scanning electron microscope (SEM). The SEM images were taken by undergraduate researcher Lauren Montemayor under my direction and supervision.

Set	C-axis speed (rev/s)	V-axis speed (mm/s)
A	0.2	0
B	1.5	0
C	0.2	5
D	0.2	0.5
E	0.2	0.1
F	1.5	0.1

Table 5.2: Sets of cutting parameters used in microwire slicing tests.

5.2.1 Slicing patterns and ease of removal

The low-magnification images of the helically sliced films, shown in Figures 5-3 and 5-4, allowed for a preliminary assessment of the instrument's performance under the different parameter settings. Parameter set A produced cutting patterns with relatively even widths of about 20 to 30 μm on both the PPy/Au and neat PPy films (Figures 5-3(a) and 5-4(a)). The widths appeared to become more uniform when parameter set B was used (Figures 5-3(b) and 5-4(b)). Both the PPy/Au and neat PPy microwires sliced with sets A and B remained adhered to the crucible and slightly adhered to neighboring lengths of wire, but the PPy/Au wires could be peeled off more easily. In general, the wires were susceptible to tearing and it was moderately difficult to remove lengths of wire longer than a few tens of millimeters.

Parameter set C produced cutting patterns that were generally more uneven and featured larger widths of about 20 to 50 μm (Figures 5-3(c) and 5-4(c)). The increased width and decreased uniformity seemed more severe in the gold-backed film. Parameter set D yielded marginal improvements over set C, but the overall result did not appear to be superior to those observed for set B (Figures 5-3(d) and 5-4(d)). The microwires sliced using sets C and D were generally less adherent to the crucible surface and neighboring lengths of wire compared to those sliced using sets A and B. They could also be removed more easily. Some sections of the wire became detached during the slicing process, as seen in Figure 5-3(d).

The cutting pattern produced using parameter set E was relatively uniform, and was similar to those of sets A and B (Figures 5-3(e) and 5-4(e)). Set F produced a slightly more uniform pattern with finer widths that appeared closer to the desired 20 μm (Figures 5-3(f) and 5-4(f)). The results appeared to be better when using a gold-backed film. Compared to the previous four parameter settings, the microwires sliced with sets E and F adhered the least to the crucible surface and adjacent lengths of wire.

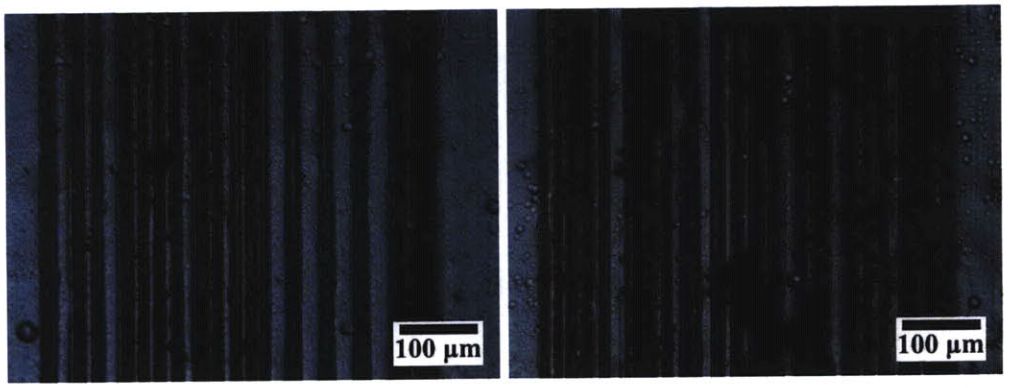

(a) Set A: low C-axis speed (neat PPy)

(b) Set B: high C-axis speed (neat PPy)

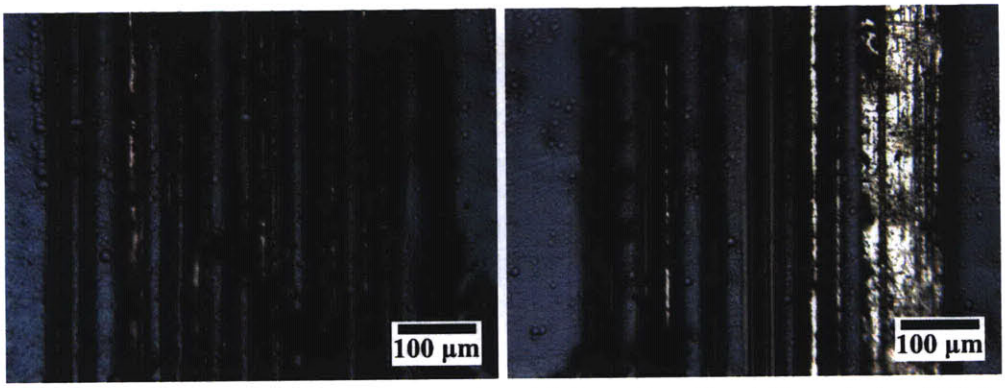

(c) Set C: low C/high V speeds (neat PPy)

(d) Set D: low C/med V speeds (neat PPy)

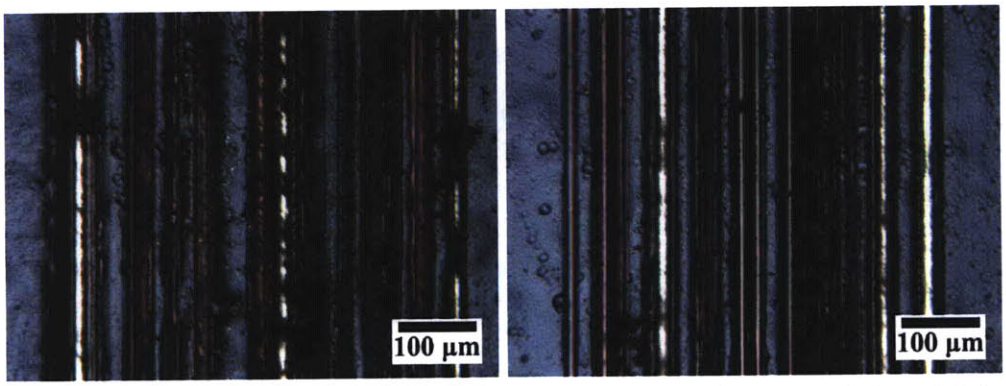

(e) Set E: low C/low V speeds (neat PPy)

(f) Set F: high C/low V speeds (neat PPy)

Figure 5-3: Optical microscope images of a neat PPy film sliced using different sets of cutting parameters. The film is still attached to the crucible. The cut starts on the right side of the image and the horizontal direction is parallel to the Z-axis.

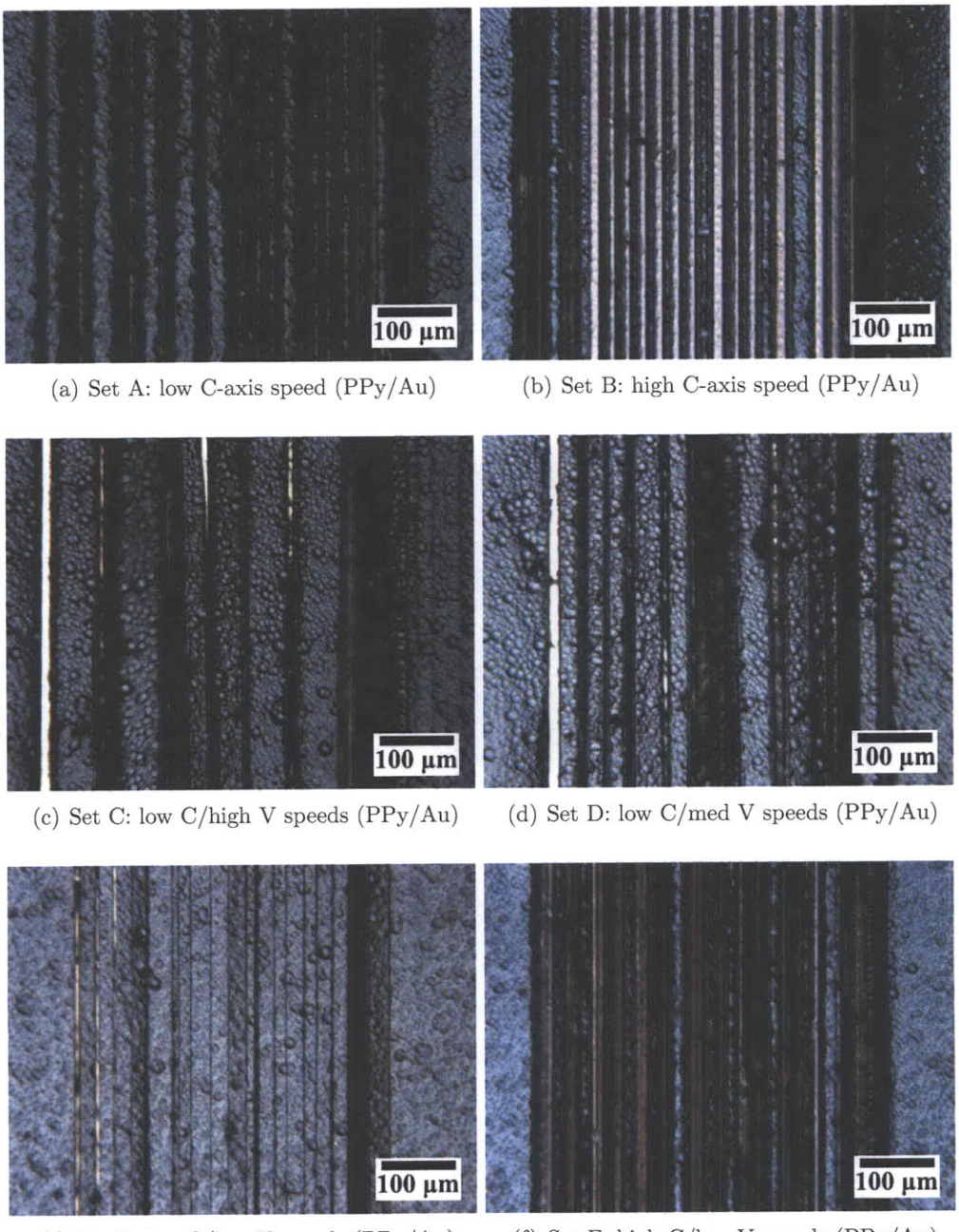

(a) Set A: low C-axis speed (PPy/Au)

(b) Set B: high C-axis speed (PPy/Au)

(c) Set C: low C/high V speeds (PPy/Au)

(d) Set D: low C/med V speeds (PPy/Au)

(e) Set E: low C/low V speeds (PPy/Au)

(f) Set F: high C/low V speeds (PPy/Au)

Figure 5-4: Optical microscope images of a gold-backed PPy film sliced using different sets of cutting parameters. The film is still attached to the crucible. The cut starts on the right side of the image and the horizontal direction is parallel to the Z-axis.

5.2.2 Wire morphology

The SEM images, shown in Figures 5-5, 5-6, 5-7, and 5-8, reveal how the morphology of the microwires is affected by the different parameter settings. The neat PPy microwires produced using parameter set A had moderate to significant ruffling on the edges and widths averaging about 23 μm (Figures 5-5(a) and 5-5(a)). Parameter set B produced finer wires about 18 μm wide with moderate ruffling, but with some visible defects (Figures 5-5(a) and 5-5(a)). In contrast, the PPy/Au wires produced using set A presented little to moderate edge ruffling and widths averaging 18 μm (Figures 5-7(a) and 5-7(a)). Using set B resulted in larger widths averaging about 25 μm and moderate edge ruffling (Figures 5-7(c) and 5-7(c)).

Parameter set C produced both neat and gold-backed PPy wires with significant edge damage (Figures 5-5(e), 5-5(f), 5-7(e) and 5-7(f)). Both types of wires were larger than the desired size and had widths ranging from about 30 to 50 μm. Using parameter set D noticeably reduced edge ruffling to moderate in both types of wires (Figures 5-6(a), 5-6(b), 5-8(a) and 5-8(b)). The neat PPy wires were sliced to an average width of about 21 μm, while the wider PPy/Au wires averaged about 25 μm.

The neat PPy microwires produced using parameter set E exhibited moderate edge damage and had an average width of about 19 μm (Figures 5-6(c) and 5-6(d)). Using set F resulted in less edge damage and the width changed little, averaging about 20 μm (Figures 5-6(e) and 5-6(f)). Similarly, the PPy/Au microwires sliced using sets E and F had widths averaging about 19 μm (Figures 5-8(c), 5-8(d), 5-8(e) and 5-8(f)). Both groups of PPy/Au wires exhibited little noticeable edge ruffling.

5.2.3 Discussion

The results described above indicate that, in general, the microwire slicing instrument is capable of producing fine wires near the desired 20 μm $\times$ 20 μm size range under the tested parameter settings. The microwires were sliced closer to the desired size and exhibited minimal edge ruffling when the V-axis was run at 0.1 mm/s and the C-axis was run at 1.5 rev/s. Both the use of a gold-backed PPy film and the sliding motion

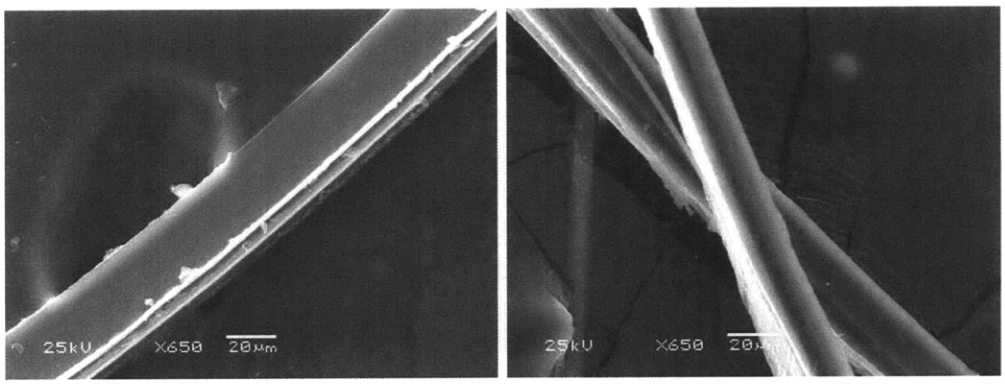

(a) Set A: low C-axis speed (neat PPy) (b) Set A: low C-axis speed (neat PPy)

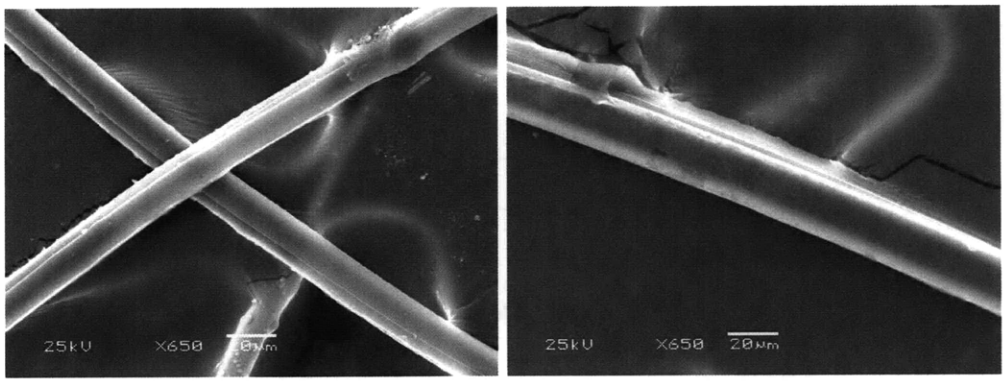

(c) Set B: high C-axis speed (neat PPy) (d) Set B: high C-axis speed (neat PPy)

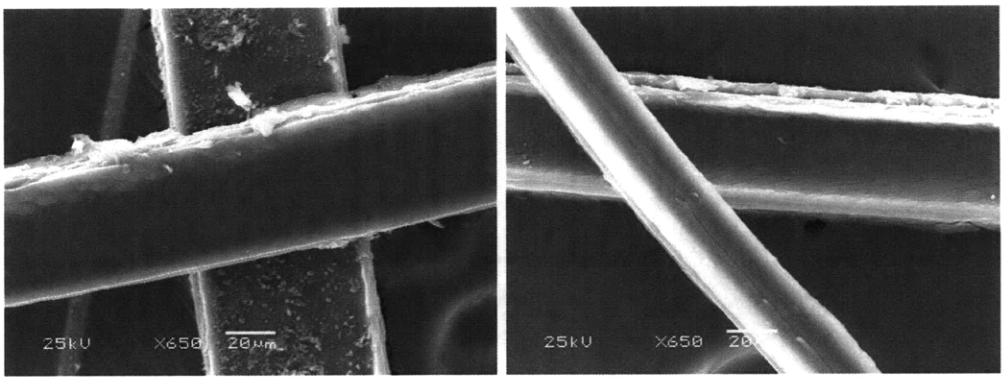

(e) Set C: low C/high V speeds (neat PPy) (f) Set C: low C/high V speeds (neat PPy)

Figure 5-5: SEM images of neat PPy microwires sliced using cutting parameter sets A, B, and C. Images taken by Lauren Montemayor.

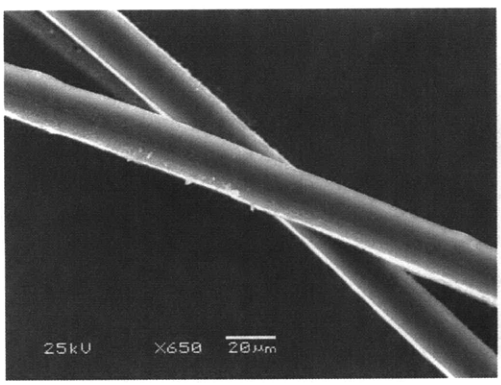

(a) Set D: low C/med V speeds (neat PPy)

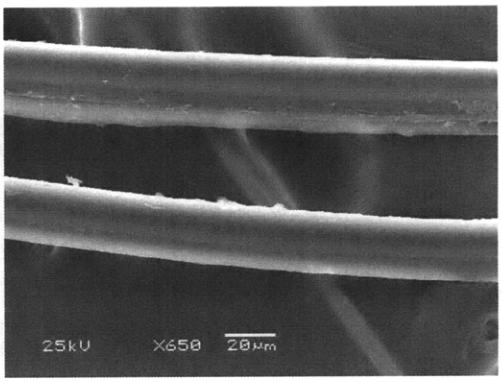

(b) Set D: low C/med V speeds (neat PPy)

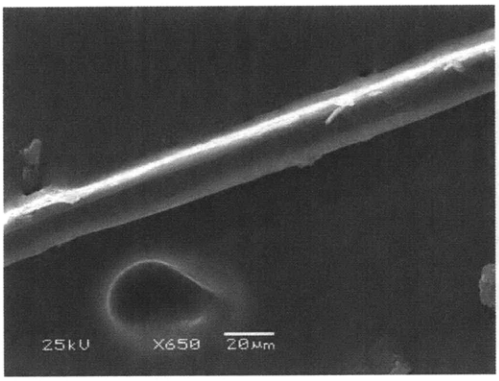

(c) Set E: low C/low V speeds (neat PPy)

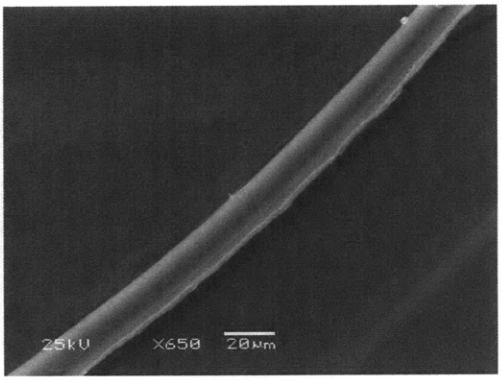

(d) Set E: low C/low V speeds (neat PPy)

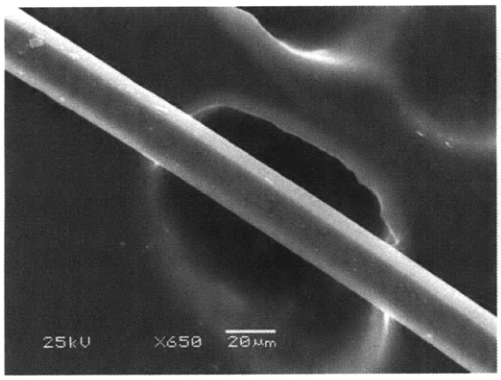

(e) Set F: high C/low V speeds (neat PPy)

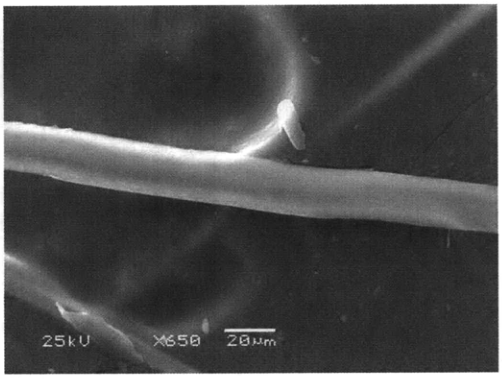

(f) Set F: high C/low V speeds (neat PPy)

Figure 5-6: SEM images of neat PPy microwires sliced using cutting parameter sets D, E, and F. Images taken by Lauren Montemayor.

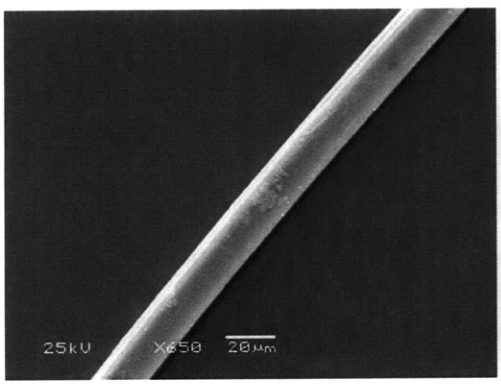

(a) Set A: low C-axis speed (PPy/Au)

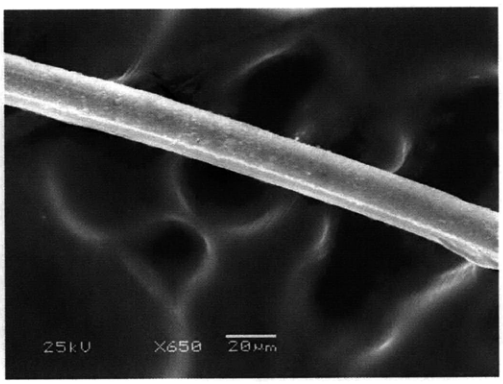

(b) Set A: low C-axis speed (PPy/Au)

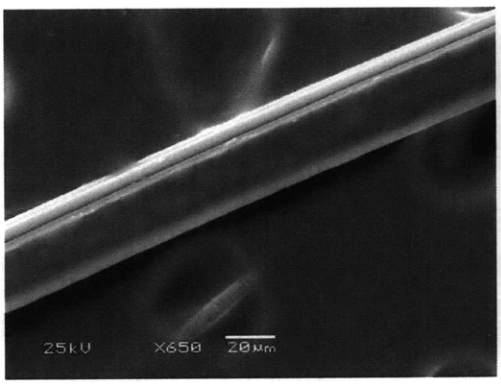

(c) Set B: high C-axis speed (PPy/Au)

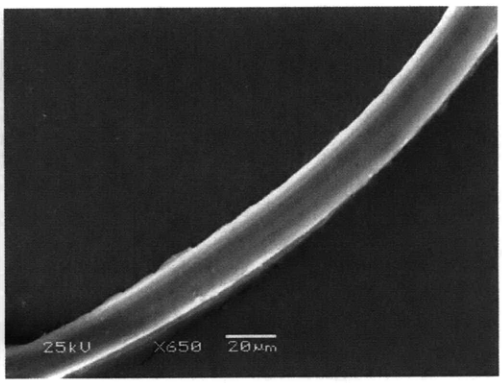

(d) Set B: high C-axis speed (PPy/Au)

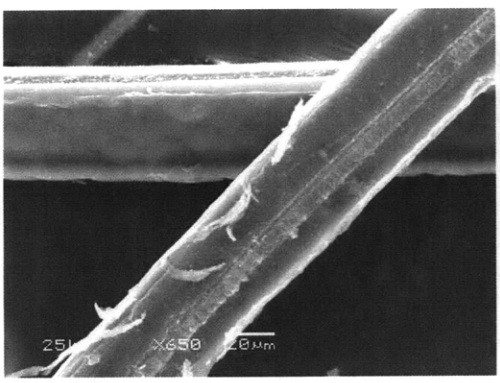

(e) Set C: low C/high V speeds (PPy/Au)

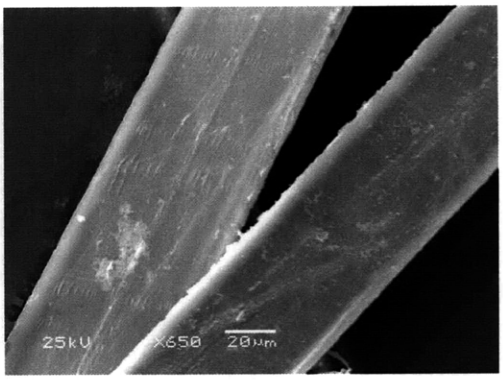

(f) Set C: low C/high V speeds (PPy/Au)

Figure 5-7: SEM images of PPy/Au microwires sliced using cutting parameter sets A, B, and C. Images taken by Lauren Montemayor.

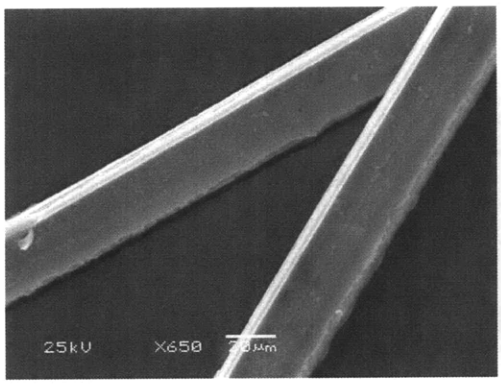

(a) Set D: low C/med V speeds (PPy/Au)

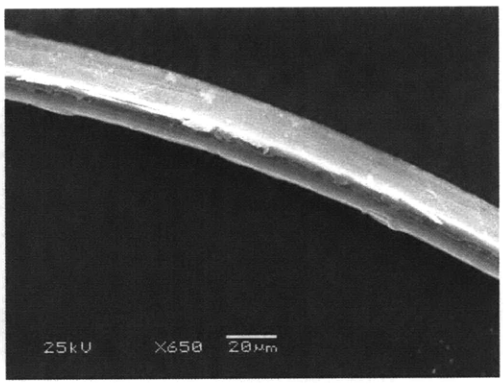

(b) Set D: low C/med V speeds (PPy/Au)

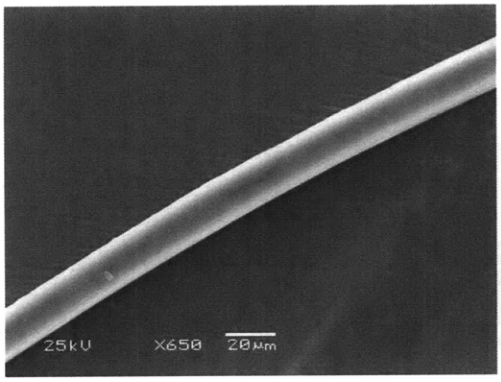

(c) Set E: low C/low V speeds (PPy/Au)

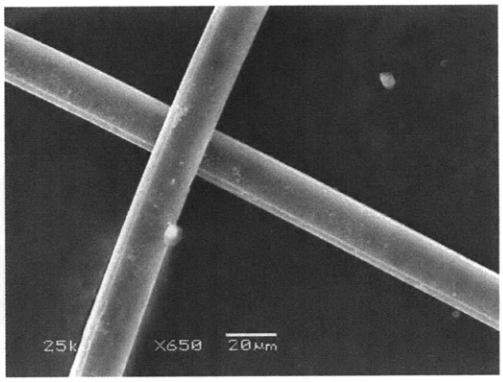

(d) Set E: low C/low V speeds (PPy/Au)

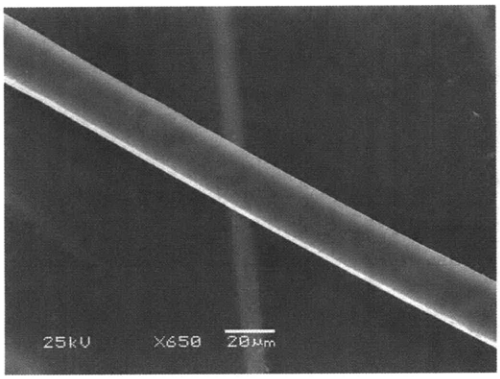

(e) Set F: high C/low V speeds (PPy/Au)

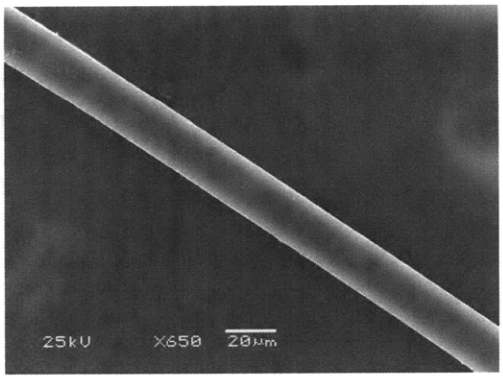

(f) Set F: high C/low V speeds (PPy/Au)

Figure 5-8: SEM images of PPy/Au microwires sliced using cutting parameter sets D, E, and F. Images taken by Lauren Montemayor.

of the V-axis were shown to help reduce the adhesion of the microwires to the crucible and adjacent lengths of wire, making it easier to remove the wires. Implemeting these optimal settings will minimize the damage caused by the cutting blade and enable the production of long, fine microwires.

5.3 Instrument Capabilities and Limitations

Additional slicing tests were conducted to fully characterize the capabilities and limitations of the microwire slicing instrument. Microwires with widths ranging from 20 to 1,000 μm were sliced from 20 μm thick gold-backed PPy films. 20 μm thick PPy-Au microwires with widths of 1,000 μm, 200 μm, 100 μm, and 20 μm are shown in Figure 5-9. Their lengths were 1.4 m, 0.9 m, 1.2 m, and 0.46 m, respectively. The first three wires were removed from the crucible using the passive wire uptake system described in Section 4.3.1. The last one was sliced using the optimal cutting parameters described in Section 5.2.3 and was carefully removed by hand. These results indicate that reducing the cross-sectional area makes it more difficult to produce long microwires.

Thinner microwires were produced by modifying the electrochemical deposition process described in Section 2.3. A PPy film 2 μm thick was grown by reducing the deposition time to 1 hour. As shown in Figure 5-10, a free-standing 2 μm $\times$ 3 μm neat PPy microwire 15 mm long was successfully cut from the film using the wire slicing instrument. The image shows some ruffling along the cut surface as was observed in the larger microwires, but overall the wire appears to be in relatively good condition. This result represents a reduction in wire cross-sectional area of two orders of magnitude (compared to a 20 μm $\times$ 20 μm cross-section) and demonstrates that the instrument is capable of producing microwires with cross-sectional dimensions of a few micrometers while minimizing damage to the material.

Further reductions in cross-sectional area and the production of sub-micrometer wires have proven difficult for two main reasons. First, as the thickness of the PPy film is reduced, it adheres more strongly to the crucible and tears easily when peeled

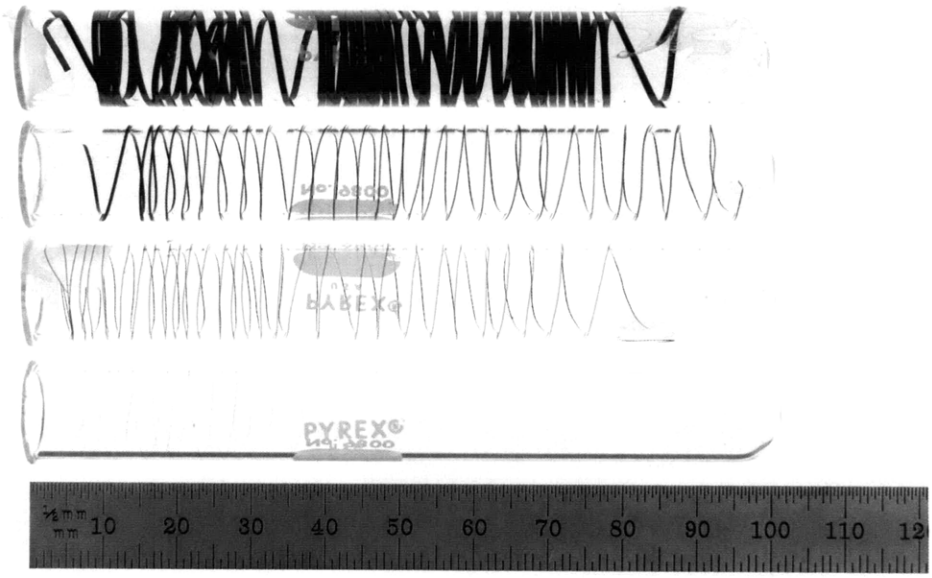

Figure 5-9: (*From top to bottom*) Gold-backed PPy microwires with 1,000 μm $\times$ 20 μm, 200 μm $\times$ 20 μm, 100 μm $\times$ 20 μm, and 20 μm $\times$ 20 μm cross-sections produced using the microwire slicing instrument. Their lengths are 1.4 m, 0.9 m, 1.2 m, and 0.46 m, respectively

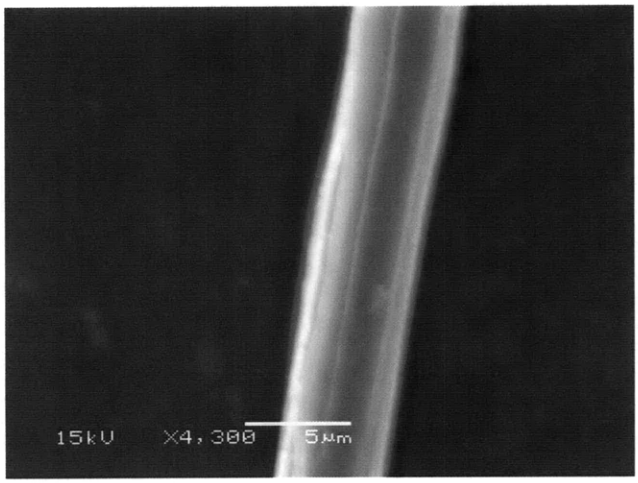

Figure 5-10: A 2 μm $\times$ 3 μm neat PPy microwire 15 mm long produced using the microwire slicing instrument.

off. PPy films less than 2 μm thick are barely free-standing, which makes it very difficult to cut and remove robust microwires. Second, sliding a cutting blade over a glassy carbon crucible is not the most appropriate method for cutting continuous microwires with cross-sectional dimensions in the 1 μm and sub-micrometer range. As the cutting edge wears, it develops a burr a few micrometers in size which makes it difficult to achieve a precise cut in the desired size range. Using a small spot size UV laser may be a better, more precise approach for cutting sub-micrometer wires.

A number of factors that limit the length of the microwires produced using the instrument were identified during testing. In general, the length of wide PPy wires (width $>$ 0.5 mm) is only limited by the size of the crucible because they are strong enough to resist tearing as they are peeled off the crucible. Thinner wires are more susceptible to tearing due to localized defects in the material and can become discontinuous due to irregularities on the crucible surface. The finer microwires, those with cross-sections of about 20 μm $\times$ 20 μm or less, also tend to peel off the crucible during the cutting operation and may become entangled on the blade. These problems may be minimized by using new or polished crucibles and by using the proposed active wire uptake system to gently and controllably peel the wire as it is cut. A problem that affects fine microwires in particular is the fact that the crucible is not a perfect cylinder and does not run true about the C-axis. The resulting wobbling motion can cause the blade to cut an irregular helical pattern and produce discontinuities along the length of the wire. This problem could be corrected by machining the crucible surface such that it rotates evenly about the C-axis.

Chapter 6

Characterization of Polypyrrole Microwires

The electrical, mechanical and electrochemical properties of conducting polymer microwires must be well understood in order to enable the incorporation of these functional materials into novel sensors and devices. An electrochemical dynamic mechanical analyzer (EDMA) developed by the Hunter Group was used to evaluate the multi-domain behavior of the PPy microwires produced using the wire slicing instrument. Microwires cut from PPy films both with gold-backing (PPy/Au) and without gold-backing (neat PPy) were tested to evaluate possible differences in performance. Static and dynamic tensile tests were performed in order to measure basic mechanical properties and characterize the dynamic compliance. The effect of strain on the resistance of the microwires was measured to demonstrate their possible use as strain gages. In addition, the microwires were incorporated into an electrochemical cell in order to evaluate their actuating performance. The following sections provide a brief description of the EDMA and the hardware modifications that enabled the testing of microwires on the device. The results of the various tests performed are presented and discussed.

6.1 The EDMA

An electrochemical dynamic mechanical analyzer, or EDMA, is an instrument used to apply a desired mechanical or electrical stimulus to a material. It is often used in the characterization of conducting polymers because it allows the user to investigate the intrinsic coupling between the mechanical and electrochemical behavior of the polymer. EDMAs have been used extensively by the Hunter Group for the characterization of conducting polymer actuators and sensors [14, 33, 38, 45, 46]. The instrument used in this work was originally fabricated by Nate Vandesteeg and Brian Schmid, and its capabilities have been further developed by Priam Pillai [38, 45].

6.1.1 System overview

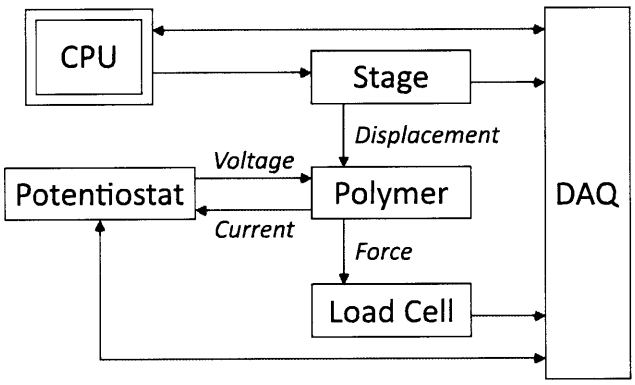

Figure 6-1: A simplified block diagram of the EDMA.

A basic block diagram of the instrument is shown in Figure 6-1. The EDMA consists of a group of instruments controlled from a desktop computer using custom Visual Basic software. The software commands a linear stage (Aerotech ALS130) driven by a motion controller (Aerotech A3200) to apply a displacement to the polymer, while a load cell (Futek LSB200) measures the resulting force. The software may also command a desired force input using a PI controller with adjustable gains. A potentiostat (AMEL 2053) applies a voltage to the polymer and measures the resulting current. A data acquisition, or DAQ, board (National Instruments BNC-2110) samples the force and displacement signals. It is also used to control the potentiostat,

and sample the voltage and current signals. The force and displacement signals are filtered by a signal conditioning amplifier (Vishay 2311) prior to sampling.

6.1.2 Modifications for microwire testing

Thin film samples characterized using the EDMA typically have length and width dimensions of a few millimeters, and are attached to the instrument using plastic or metal clamps. Microwires cannot be secured properly using these clamps and tend to slip out easily. Therefore, new attachment hardware based on 26 gauge (0.457 mm) syringe needles (Becton Dickinson) was fabricated, as shown in Figure 6-2. An adjustable optic holder (Linos Microbench) was attached to the linear stage and fitted with a conical connector onto which a needle is securely press-fit. A second needle was pressed and glued into a laser-cut acrylic part, which was then bolted onto the load cell. The needles can be aligned in the vertical and lateral directions using the positioning knobs on the optic holder.

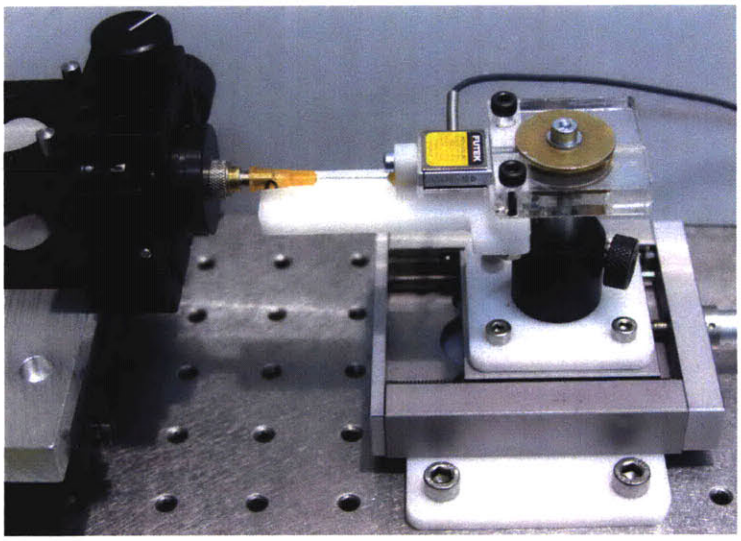

Figure 6-2: EDMA with syringe needles used for attaching microwires. The needle on the left is mounted on the adjustable optic holder and the one on the right is attached to the load cell.

The static and dynamic tensile testing conducted in this work did not require electrical connections between the microwire sample and the potentiostat. This al-

lowed for a simple attachment method in which the ends of the microwire were glued onto the tips of the needles using UV cure adhesive (Loctite 356). The adhesive was exposed to UV light for 2 minutes using a light curing system (Electro-Lite Corp. ELC-405) and allowed to cure overnight. Once the microwire was attached to the pair of needles, it was loaded onto the EDMA for testing, as shown in Figure 6-3. Before starting the test, the needle tips were brought together until they were barely touching in order to set the zero position. The load cell was attached to a manual linear stage (Linos TB 80-25) to facilitate this process. The length of the wires was then measured using the instrument's built-in sample measuring routine, which pulled the needle tips apart until the wire was brought into slight tension ($\sim$1 mN).

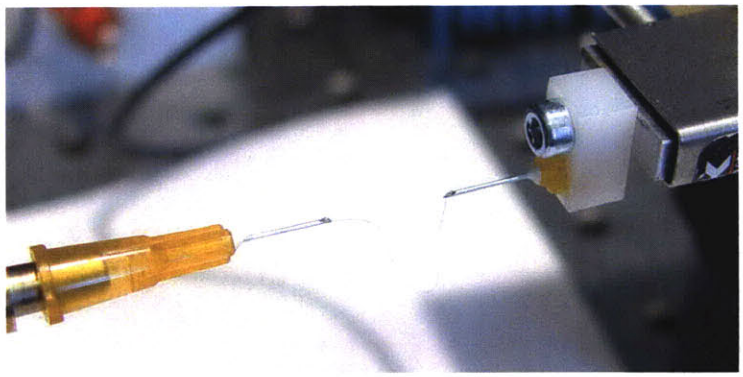

Figure 6-3: A PPy microwire glued to the needle tips and loaded onto the EDMA for testing.

Measurements of the strain-resistance relationship required that the microwire be electrically connected to the potentiostat. Therefore, a different attachment method was employed, as shown in Figure 6-4. A short length of 32 gauge (0.229 mm) hypodermic tubing (Small Parts) was inserted into each needle, and its end was bent in order to secure it in place and establish an electrical connection with the needle. The tubing was then crimped over the ends of the microwire. In order to measure resistance without applying a significant force to the needles, thin 40 AWG (0.079 mm) bare copper electrical wire was tightly wound around each needle and glued into place. Once the sample was loaded onto the EDMA, the ends of the copper wire were connected to the potentiostat.

This attachment method provides a two-wire resistance measurement. A four-wire measurement is typically used in order to reduce the effect of contact resistance, but proved difficult to implement effectively. Nonetheless, the effect of contact resistance should be minimal since the approximately 2 Ω resistance between the copper wire and the hypodermic tubing is negligible compared to the few kilohm resistance of the microwire.

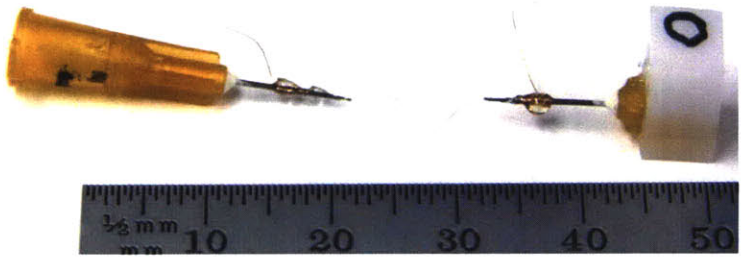

Figure 6-4: A PPy microwire prepared for strain-resistance measurements.

During the electrochemical actuation tests, the microwires acted as the working electrode in an electrochemical cell, and were electrically connected to the potentiostat using the attachment described above. An open-ended glassy carbon bath 2 mm wide, 2 mm deep, and 18 mm long was fabricated using a wire EDM, and filled with ionic liquid. As shown in Figure 6-5, this bath geometry allowed for the wire to be submerged in the ionic liquid without also submerging the syringe needles, thus preventing undesired electrochemical reactions. A silver wire placed in close proximity to the PPy microwire was used as the reference electrode, and the bath served as the counter electrode. The bath was connected to a miniature three-axis manual stage (Newport M-DS25) to allow for fine position adjustments. In practice, the stage-mounted bath was first lowered and slid under the wire, and then raised upwards until the wire was submerged.

6.2 Static Tensile Tests

Static tensile tests were performed in order to obtain experimental measurements of a PPy microwire's basic mechanical properties. Microwires about 20 μm wide

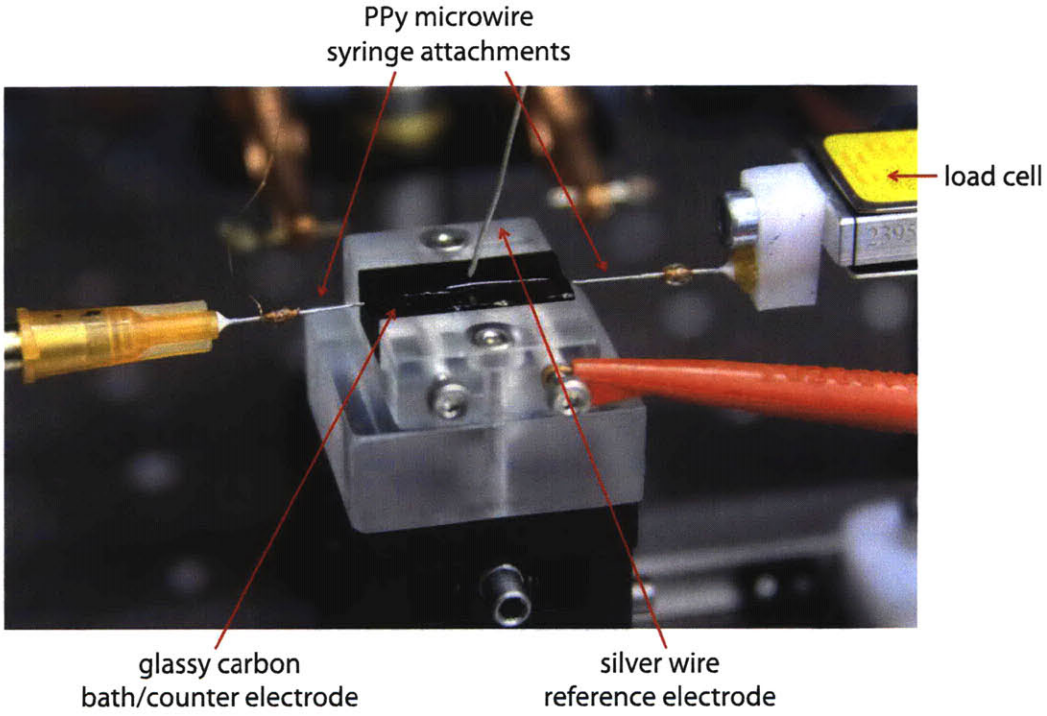

Figure 6-5: A PPy microwire submerged in ionic liquid during actuation. Surface tension prevents the liquid from dripping out of the glassy carbon bath.

were sliced from 20 μm thick PPy films with and without gold-backing using the wire slicing instrument. The wires were cut and tested within a week of the films' electrodeposition. A total of eleven PPy/Au wire samples were collected, including three wires about 10 mm long, three about 20 mm long, three about 30 mm long, and two about 40 mm long. A total of nine neat PPy wires were collected, including three wires about 10 mm long, three about 20 mm long, and three about 30 mm long.

The wire samples were prepared and loaded on the EDMA as described in Section 6.1.2. Once the sample length was measured, the sample was stretched at a constant strain rate of 0.5 %/s until failure. These static tensile tests were conducted by undergraduate researcher Lauren Montemayor under my direction and supervision.

Force and strain data were collected and analyzed for each sample. A typical force-strain measurement is shown in Figure 6-6. Force was used instead of stress because the cross-sectional areas of the wires were not measured. The length, stiffness, yield force, failure force, and final strain were recorded for each sample. The yield force was calculated using the 0.2% yield criterion.

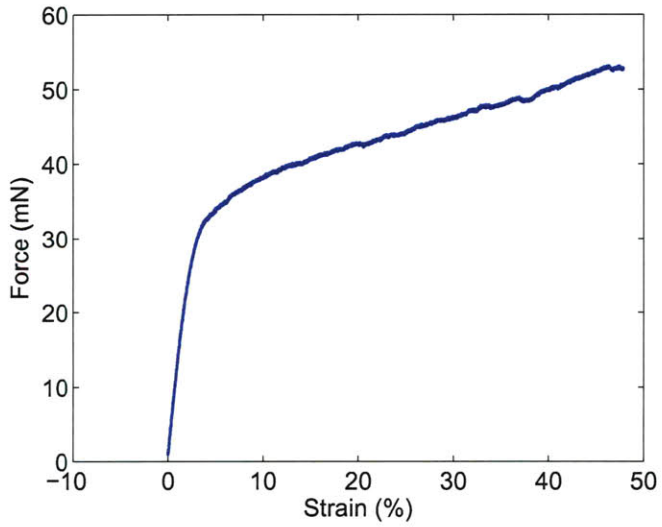

Figure 6-6: A typical measured force-strain curve. The sample is a PPy/Au microwire 30.3 mm long with a cross-sectional area of approximately 20 μm $\times$ 20 μm.

The PPy/Au wires yielded at an average force of 20.5 $\pm$ 5.6 mN, with the stiffer wires yielding at slightly higher forces. The failure force averaged 43.7 $\pm$ 11.7 mN,

and the final strain varied from 12.1% to 69.3%, averaging 44.6 ± 21.7%.

The neat PPy wires yielded at an average force of 14.7 ± 5.9 mN, with the stiffer wires yielding at slightly higher forces. The force at failure averaged 33.4 ± 14.9 mN, and the final strain varied from 30.2% to 69.4%, averaging 49.5 ± 14.8%.

The measured stiffness for both types of PPy microwires was found to decrease with sample length. This is to be expected since stiffness is inversely proportional to sample length. It can be reasonably assumed from previous observations that the cross-sectional area ranges from 20 μm × 20 μm to 30 μm × 30 μm, and that the polymer's elastic modulus is about 1.4 GPa. Based on these assumptions, the measured stiffness values fall within the expected range given possible variations in cross-sectional area, as shown in Figure 6-7.

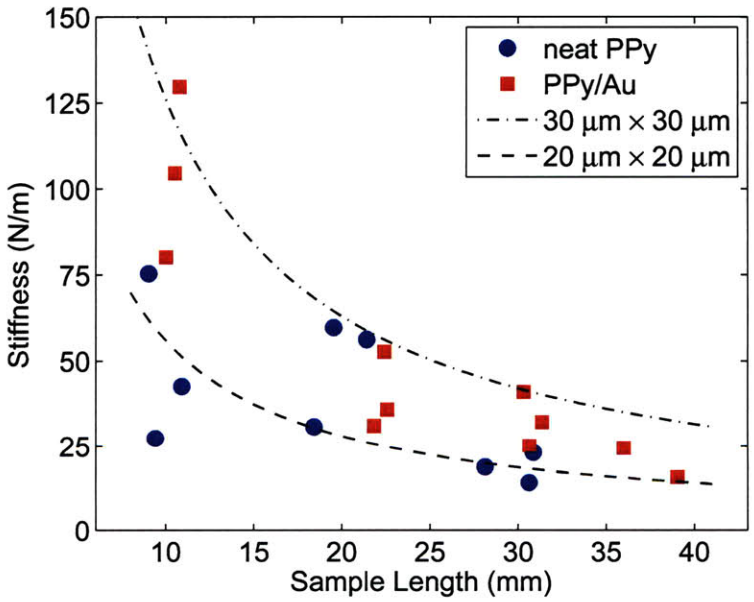

Figure 6-7: Measured Stiffness vs. Sample Length. Cross sections of 30 μm × 30 μm and 20 μm × 20 μm are assumed for the top and bottom dashed curves, respectively. A Young's Modulus of 1.4 GPa is assumed.

These results show that the addition of a fine gold backing does not have a significant effect on the mechanical behavior of PPy microwires. The measured mechanical properties are comparable to those obtained from the tensile testing of thin PPy films.

Variations between samples are likely due to localized defects and slight differences in cross-sectional area.

6.3 Characterization of Dynamic Compliance

Recent work by the Hunter Group has focused on the characterization of the dynamic compliance of conducting polymers through the use of stochastic linear system identification techniques [33, 34]. These powerful techniques allow for the development of mathematical models of systems using measured data of inputs, outputs, and noise in the system.

In the case of a single input single output (SISO) system, the output y results from the convolution of the input x with the function f as represented in the equation,

$$y_i = \sum_{j}^{N} h(j)x(i-j), \tag{6.1}$$

where *h(j)* is the impulse response function. This function can be estimated from measured system inputs and outputs by computing and mathematically manipulating their corresponding auto and cross-correlation functions. The impulse response uniquely characterizes the system response for any input and can be used to obtain system parameters such as the natural frequency, damping ratio and DC gain. For the tests performed in this work, the impulse response represents the compliance of the PPy microwire and dictates the displacement resulting from an applied force. A Gaussian white noise input may used to elicit the dynamic response over a range of frequencies in a single test.

Once the linear model has been estimated, the quality of the system identification procedure can be evaluated using the coherence squared function (γ^2). $\gamma^2 = 1$ indicates that the response is linear while $\gamma^2 < 1$ indicates the presence of noise and nonlinearities in the system as a function of frequency. Another indicator of the model's ability to predict the system output is the variance accounted for (VAF). It

is given by the equation

$$VAF = 100\left(1 - \frac{\sigma(y_{est_i} - y_i)^2}{\sigma(y_i)^2}\right), \tag{6.2}$$

where y_{est} is the predicted output, y is the measured output, and $\sigma(y)$ is the standard deviation. For a detailed discussion of system identification and the coherence function please refer to [22].

Dynamic tests were performed on microwires with lengths of about 20 mm and cross-sectional areas of about 20 μm $\times$ 20 μm, which were cut from PPy films both with and without gold-backing. Using the EDMA, the wires were subjected to a Gaussian force input with an average force of 19.7 mN and standard deviation of 2.7 mN. This force range was chosen in order to prevent buckling and remain within the polymer's linear viscoelastic region. The input power bandwidth was limited to 100 Hz by the capabilities of the linear stage and the low-pass filtering performed by the signal conditioning amplifier, as shown in Figure 6-8(a). In order to achieve the desired input forces without destabilizing the stage, the force PI controller gains K_p and K_i were kept at or below 9,000 and 400, respectively. The tests were conducted for 50 seconds with a sampling frequency of 3 kHz, and the measured data was low-pass filtered at 100 Hz and detrended before applying the linear analysis.

Typical dynamic test data for a neat PPy microwire is shown in Figure 6-8. The coherence estimate of the compliance was nearly unity and decreased significantly after 100 Hz, as shown in Figure 6-8(b). This corresponds with the input power bandwidth and indicates that the estimated responses are linear for frequencies up to 100 Hz. Figure 6-8(c) shows the estimated compliance frequency response. The compliance values at low frequencies were in agreement with the values reported in Section 6.2. The compliance impulse response function was estimated with a time resolution of 0.33 milliseconds, as shown in Figure 6-8(d). Using measured data not used for model estimation, the estimated impulse response functions were shown to be good predictors of the output with the VAF generally between 93% and 97%.

These results demonstrate the successful identification of the compliance frequency

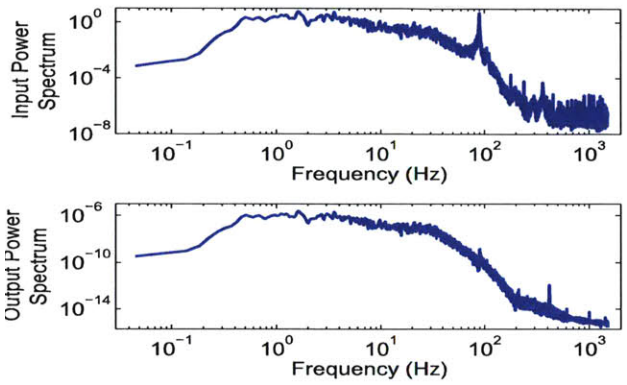

(a) Force and strain power spectrums

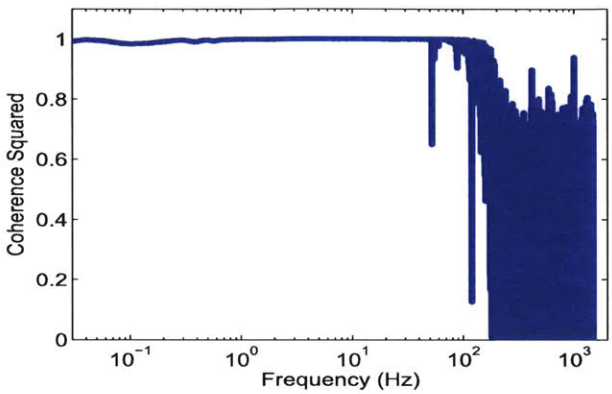

(b) Coherence squared estimate

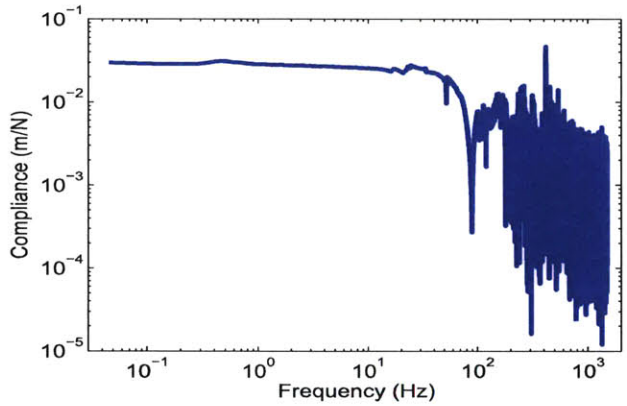

(c) Compliance frequency response

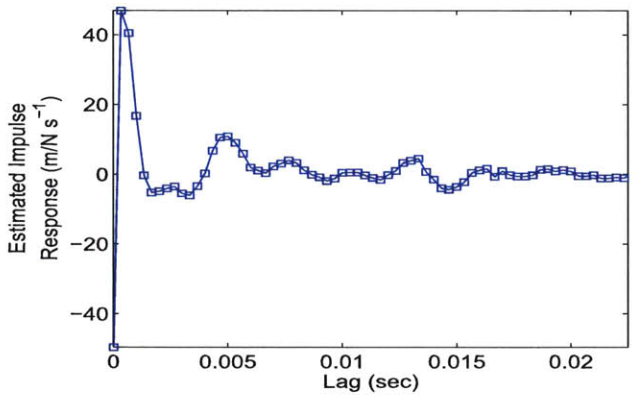

(d) Compliance impulse response

re 6-8: Typical dynamic test data for a neat PPy microwire. **(a)** The input and output power spectrums. The input · bandwidth is limited to 100 Hz. **(b)** The coherence squared estimate of the compliance. It indicates that the estimated ıses are linear for frequencies up to 100 Hz. **(c)** The compliance frequency response. The compliance is stable at low encies and rolls off after 100 Hz. **(d)** The compliance impulse response function. It was estimated by applying a Gaussian input and sampling at 3 kHz.

and impulse responses of PPy microwires using the EDMA. No significant difference was observed between the results for neat PPy and PPy/Au wires. The estimated compliance frequency responses were comparable to responses obtained for PPy films [34]. The estimated compliance impulse responses, despite being good predictors of the output, were not as well resolved as those estimated for films [34]. This is most likely due to the fact that the measured forces are low and close to the noise floor of the load cell.

6.4 Strain-Resistance Relationship

Experimental measurements of the strain-resistance relationship of PPy microwires are an important step in determining their use in position sensing applications. The Hunter Group has previously created strain sensors using PPy-coated fabrics and PPy films with gage factors ranging from 2 to 10 [29, 46]. The gage factor GF is defined as

$$GF = \frac{\Delta R/R_G}{\epsilon}, \tag{6.3}$$

where R_G is the resistance of the undeformed strain gage, ΔR is the change in resistance resulting from the strain, and ϵ is the applied strain. Based on previous results for PPy films and simple theory, the resistance is expected to increase linearly with strain. The resistance R of a wire can be modeled as

$$R = \frac{L}{\sigma A}, \tag{6.4}$$

where σ is the conductivity of the material, L is the wire length, and A is the cross-sectional area. When a strain is applied, the simultaneous increase in length and decrease in cross-sectional area results in an increase in resistance. The conductivity is assumed to remain constant for the applied strains.

Microwire samples with lengths of about 20 mm and cross-sectional areas of about 20 μm $\times$ 20 μm were cut from PPy films both with and without gold-backing using the wire slicing instrument. The wires were loaded onto the EDMA and connected to the

potentiostat using the apparatus described in Section 6.1.2. The wire resistance was measured by applying a 2 V potential and measuring the resulting current. Sinusoidal strain inputs with a frequency of 0.1 Hz and amplitudes of 1 to 5% were applied for up to 100 seconds. Before testing, an 8 to 12 mN preload was applied in order to prevent the wire from buckling due to creep.

The PPy/Au wires generally had resistances of about 2 kΩ to 4 kΩ at their undeformed length, which corresponded to conductivities of about 16,370 S/m to 28,750 S/m. Their resistance increased linearly with strain and responded consistently throughout the test, as shown in Figure 6-9. These changes in resistance corresponded to a gage factor of about 0.7.

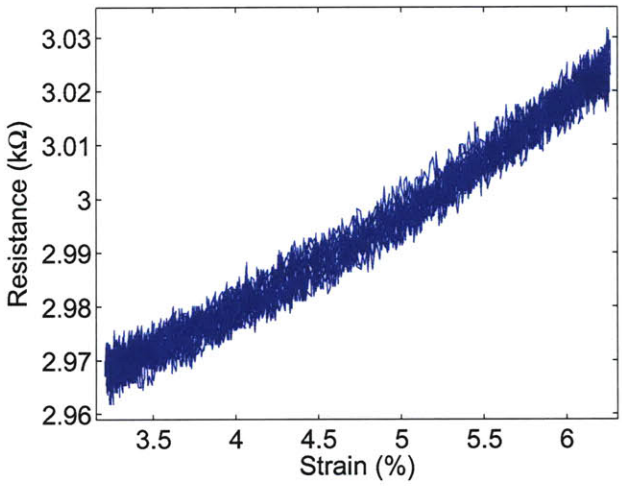

Figure 6-9: Strain-resistance response for a 20.3 mm long PPy/Au microwire. The input was a 3% strain sinusoid at 0.1 Hz. The changes in resistance are relatively consistent over time and correspond to a gage factor of about 0.7.

The neat PPy microwires typically had resistances of about 2.5 kΩ to 8 kΩ at their undeformed length, which corresponded to conductivities of about 5,720 S/m to 19,000 S/m. Their resistance generally increased linearly with strain, with most of the samples exhibiting an upwards drift in resistance over time. This behavior was observed with various degrees of severity as shown in Figure 6-10. A gage factor of about 0.4 was computed for samples in which the drift was negligible.

The creep response of the wires prevented the application of strain amplitudes

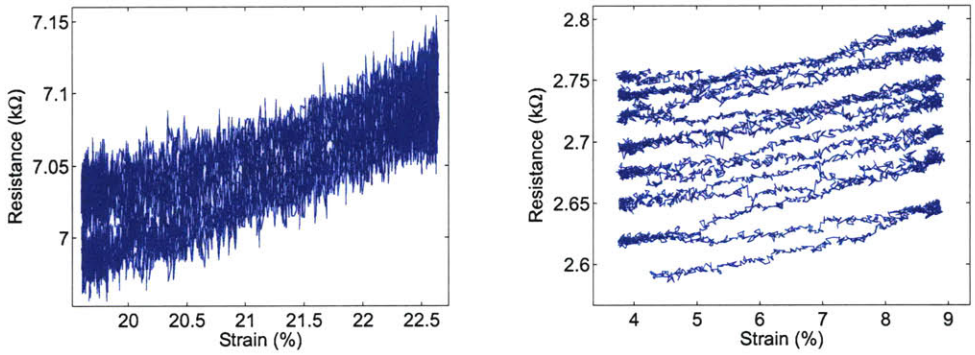

Figure 6-10: (*Left*) Strain-resistance response for a 21.7 mm long neat PPy microwire. The input was a 3% strain sinusoid at 0.1 Hz. The change in resistance remains fairly constant with time and corresponds to a gage factor of about 0.4. (*Right*) Response for a 13.4 mm long neat PPy microwire. The input was a 5% strain sinusoid at 0.1 Hz. The resistance drifts upwards significantly over time.

larger than 5% at 0.1 Hz. In order to investigate the response to larger strains, an 8% strain at 1 Hz was applied to a PPy/Au microwire. The measured response, shown in Figure 6-11, was consistent over time and suggests that the strain-resistance relationship is nonlinear at higher strain amplitudes.

These results demonstrate that the resistance-strain relationship of PPy microwires can be modeled as linear for strain amplitudes up to 5% and frequencies up to 0.1 Hz. The microwires begin to exhibit nonlinear behavior at 8% strain. It is believed that the increase in resistance over time observed for the neat PPy microwires may be related to the creep response of the polymer, and that the addition of a gold layer possibly helps diminish this effect. Further testing, along with more detailed modeling of the effects of deformation on the wire resistance, may be required to more adequately characterize this behavior.

6.5 Electrochemical Actuation

Cyclic voltammetry experiments were performed in order to evaluate the electroactivity and actuation performance of the PPy microwires. Microwire samples with lengths of about 20 mm and cross-sectional areas of about 20 μm $\times$ 20 μm were cut from

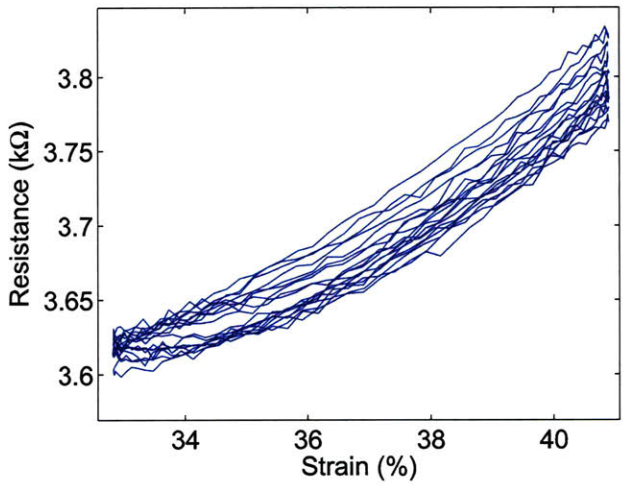

Figure 6-11: Strain-resistance response for a 20.3 mm long PPy/Au microwire. The input was a 8% strain sinusoid at 1 Hz.

PPy films both with and without gold-backing using the wire slicing instrument. The wires were loaded onto the EDMA and incorporated into an electrochemical cell, as described in Section 6.1.2. $BMIMPF_6$ (Solvent Innovation) was used as the electrolyte solution.

Three types of experiments were conducted on each sample in the same order. First, a ± 1 V (versus reference) triangle wave at 50 mVs^{-1} was applied in order to obtain a cyclic voltammogram. This was followed by isotonic testing during which a 0.05 Hz ± 1 V square wave and a 0.8 mN preload were applied. The 20 cycle isotonic test was preceded by a 40 cycle warmup. Finally, isometric testing was conducted by applying a 0.05 Hz ± 1 V square wave. The 20 cycle isometric test was preceded by a 20 cycle warmup. The isotonic strains and isometric forces recorded during actuation were low-pass filtered using a 10 Hz cutoff frequency in order to reduce measurement noise.

The cyclic voltammograms for a 19.2 mm long PPy/Au wire and a 19.5 mm long neat PPy wire are presented in Figure 6-12(a). They show that the redox response of the PPy/Au wires is significantly more pronounced than that of the neat PPy wires. Also of note, the PPy/Au wires were found to exhibit atypical behavior during the

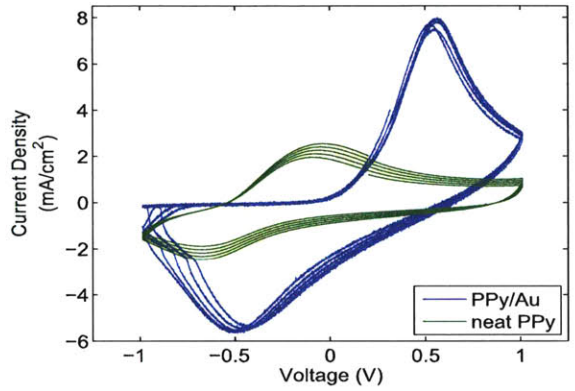

(a) Cyclic voltammograms

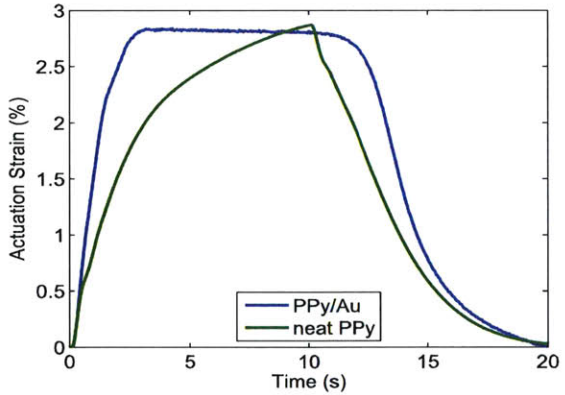

(b) Isotonic strain response

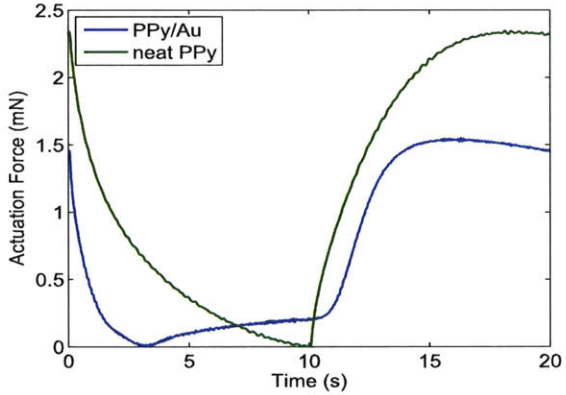

(c) Isometric force response

Figure 6-12: Typical responses for both neat PPy and PPy/Au microwires during cyclic voltammetry in $BMIMPF_6$. **(a)** Cyclic voltamograms between -1 V and +1 V (versus reference) at 50 mVs^{-1}. **(b)** Isotonic strains averaged over 10 actuation cycles. A 0.05 Hz ± 1 V square wave and a 0.8 mN preload were applied. **(c)** Isometric forces averaged over 10 cycles. A 0.05 Hz ± 1 V square wave was applied.

reduction phase of the cycle from about 0 V to -1 V. After the first few cycles, the wire behaves much like a diode in that the current effectively remains at zero despite changes in voltage.

The isotonic strains recorded for these wires are shown in Figure 6-12(b). The PPy/Au wire produced a strain output of 2.8%, and acheived peak strain rates of 2.3%/s and -0.9%/s during oxidation and reduction, respectively. The neat PPy wire produced a strain output of 2.9%, and acheived peak strain rates of 1.7%/s and -0.6%/s during oxidation and reduction, respectively. The measured isometric forces are shown in Figure 6-12(c). The PPy/Au wire produced a force output of 1.5 mN, and acheived peak force rates of -3.1 mN/s and 0.6 mN/s during oxidation and reduction, respectively. The neat PPy wire produced a force output of 2.3 mN, and acheived peak force rates of -2.4 mN/s and 1.7 mN/s during oxidation and reduction, respectively.

The measured actuation performance is in agreement with previous actuation studies of PPy films, and demonstrates that PPy microwires are capable of producing useful amounts of strain and force. These results indicate that the incorporation of the conducting gold layer accelerates the propagation of charge along the length of the actuator. This is evidenced by the higher strain and stress rates achieved by the PPy/Au microwires in comparison to the the neat PPy wires. The addition of the gold layer did not increase the actuation strain and force as was shown in previous studies of gold-backed PPy films [14].

Chapter 7

Conclusions and Future Work

7.1 The Microwire Slicing Instrument

A computer-controlled, four-axis instrument was developed for slicing long, fine microwires from PPy films electrodeposited on a glassy carbon crucible. The effects of different operating parameter settings on blade wear and wire morphology were characterized through extensive testing. It was determined that the best results were achieved when the V-axis was run at 0.1 mm/s, the C-axis was run at 1.5 rev/s, and the film had a thin layer of gold on the side facing the crucible. The current capabilities of the device and the factors limiting the production of fine microwires several meters in length were also discussed.

In its current state, the wire slicing instrument lacks a mechanism for removing the PPy microwire from the crucible after it is cut. A passive wire uptake system was developed and shown to effectively remove wires as thin as 100 μm $\times$ 20 μm. These results suggest that an active sytem capable of applying low tensions in a controlled manner would be required to remove fine 20 μm $\times$ 20 μm wires. A design for an active wire uptake system that spools the microwire with constant tension was described in Section 4.3.2. A miniature DC motor (Portescap 08G61) capable of producing the small torques required has been selected and purchased, as well as two high resolution optical rotary encoders (Avago AEAS-7000). The detailed engineering for the proposed design must still be done, particularly the design of the

spring element located between the motor and the spool. A control system must also be developed to set the angle difference, and thus the tension, using the DC motor.

7.2 Characterization of Polypyrrole Microwires

The electrical, mechanical and electrochemical properties of PPy microwires were successfully characterized using the EDMA. Basic mechanical properties including stiffness, yield force, failure force, and final strain were measured experimentally. The compliance frequency and impulse responses were estimated from dynamic tests using a Gaussian force input, and the latter were shown to be good predictors of the system output. The PPy microwires were shown to have high conductivities and their strain-resistance relationship was found to be relatively linear for modest strains. In addition, it was demonstrated that the microwires are capable of producing useful amounts of strain and force during electrochemical actuation. These results demonstrate that PPy microwires produced by slicing electrodeposited PPy films are suitable for applications such as smart textiles, high fidelity neural recording, micro-actuation, and flexible polymer-based electronics.

This thesis lays the groundwork for further characterization of the mechanical and electrochemical behavior of PPy microwires. The microwires may be subjected to simultaneous mechanical and electrical inputs in order to determine the effect of charge on the dynamic compliance of the polymer. Also, multiple microwires may be bundled or braided together and actuated in parallel to produce higher forces. Another interesting possibility is to incorporate carbon nanotubes into the microwires, and investigate their effect on actuation performance and mechanical properties.

7.3 Production of Fabrics Using Polypyrrole Microwires

Individual textile fibers are typically spun together to produce a continuous thread or yarn. Over the past year, we have been collaborating with Dr. Carole Winterhalter

of the US Army Natick Research Development and Engineering Center to produce conductive fabrics made from PPy microwires. Dr. Winterhalter has inspected 20 μm $\times$ 20 μm microwires produced using the microwire slicing instrument and has determined that they can be spun into a thread. She has indicated that the microwires should all be about 25 mm long in order to achieve the best results. The next step in this collaboration involves more detailed testing of the microwires by Dr. Winterhalter's colleagues at North Carolina State University. The goal is to determine how well they can be spun and blended with other textile fibers.

Appendix A

Spindle Part Drawings

The following pages contain detailed drawings for the bearing block and shaft used in the spindle of the wire cutting instrument. These drawings were provided to the MIT Central Machine Shop and all dimensions are specified in inches. The bearing block is designed to house two 20 mm bore diameter ABEC-3 angular contact bearings (SKF 7204 BEP). The shaft is secured and preloaded with a .664"-32 thread locknut (Whittet-Higgins Co.) and disc springs (Schnorr Corp. K6001). This spindle design provides adequate stiffness for applications with moderate spindle speeds and shaft loads.

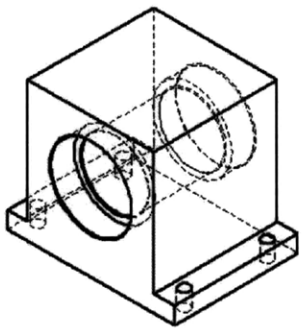

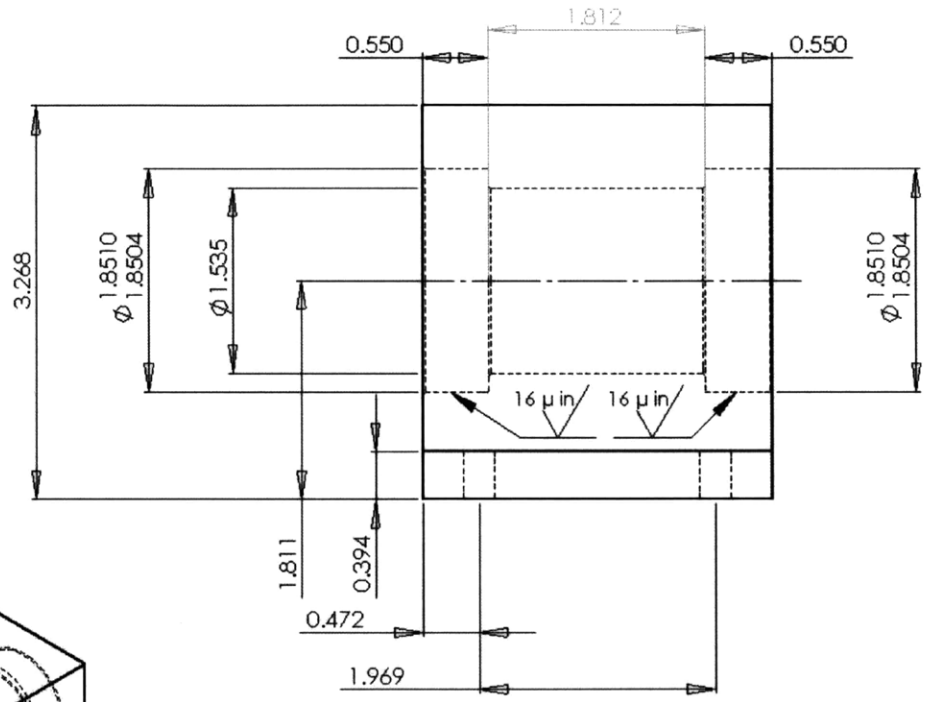

UNLESS OTHERWISE SPECIFIED:

All dimensions in inches

Tolerances are ± 0.005

MATERIAL: Steel

Contact: Miguel Saez masaez@mit.edu

TITLE: Bearing Block (Side View)

SCALE: 1:1

SHEET 1 OF 4

5 4 3 2 1

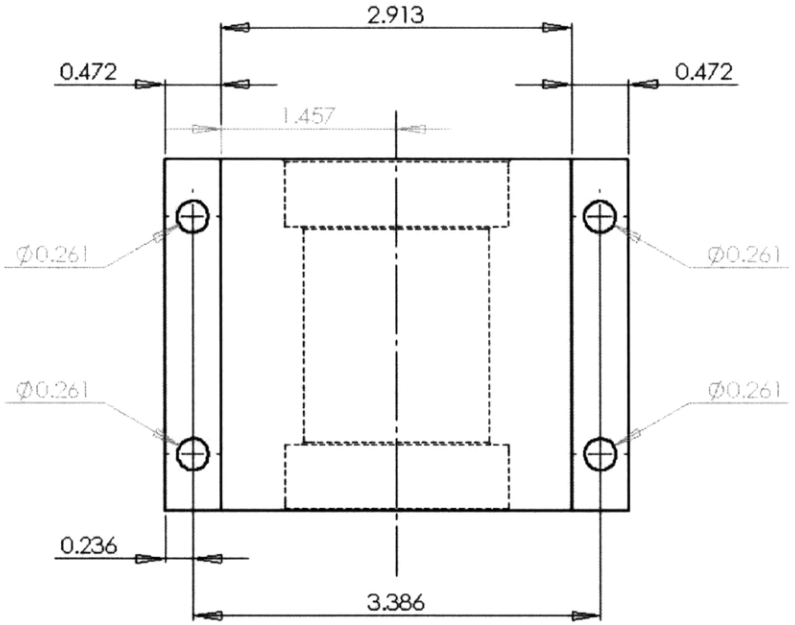

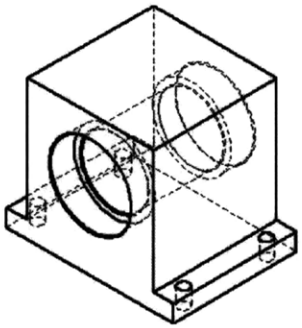

UNLESS OTHERWISE SPECIFIED:

All dimensions in inches

Tolerances are ± 0.005

MATERIAL: Steel

Contact: Miguel Saez masaez@mit.edu

TITLE: Bearing Block (Top View)

SCALE: 1:1

SHEET 2 OF 4

5 4 3 2 1

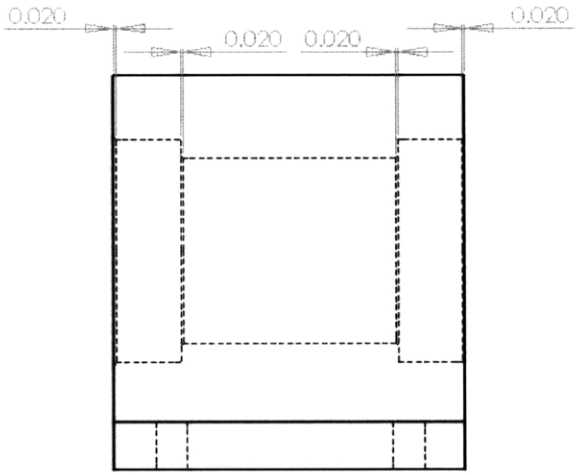

Note: All chamfers are 45° unless otherwise specified.

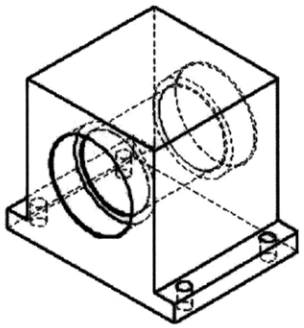

UNLESS OTHERWISE SPECIFIED:

All dimensions in inches

Tolerances are ± 0.005

MATERIAL: Steel

Contact: Miguel Saez masaez@mit.edu

TITLE:

Bearing Block (Side View)

Chamfer locations

SCALE: 1:1

SHEET 3 OF 4

5 4 3 2 1

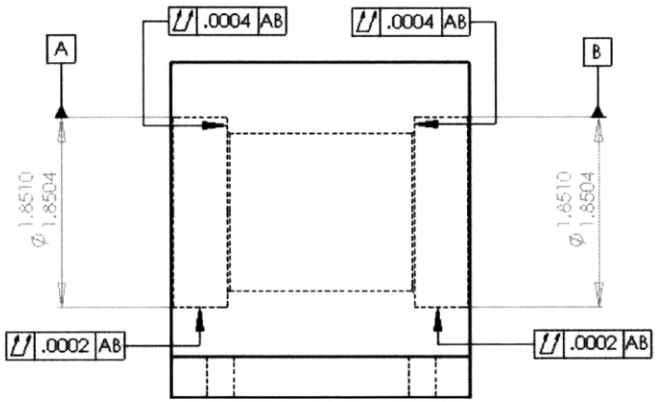

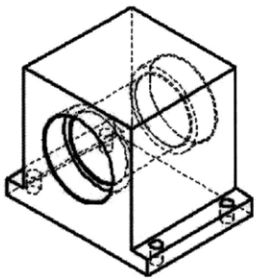

UNLESS OTHERWISE SPECIFIED:

All dimensions in inches

Tolerances are ± 0.005

MATERIAL: Steel

Contact: Miguel Saez masaez@mit.edu

TITLE:

Bearing Block (Side View)

Form tolerances

SCALE: 1:1

SHEET 4 OF 4

5 4 3 2 1

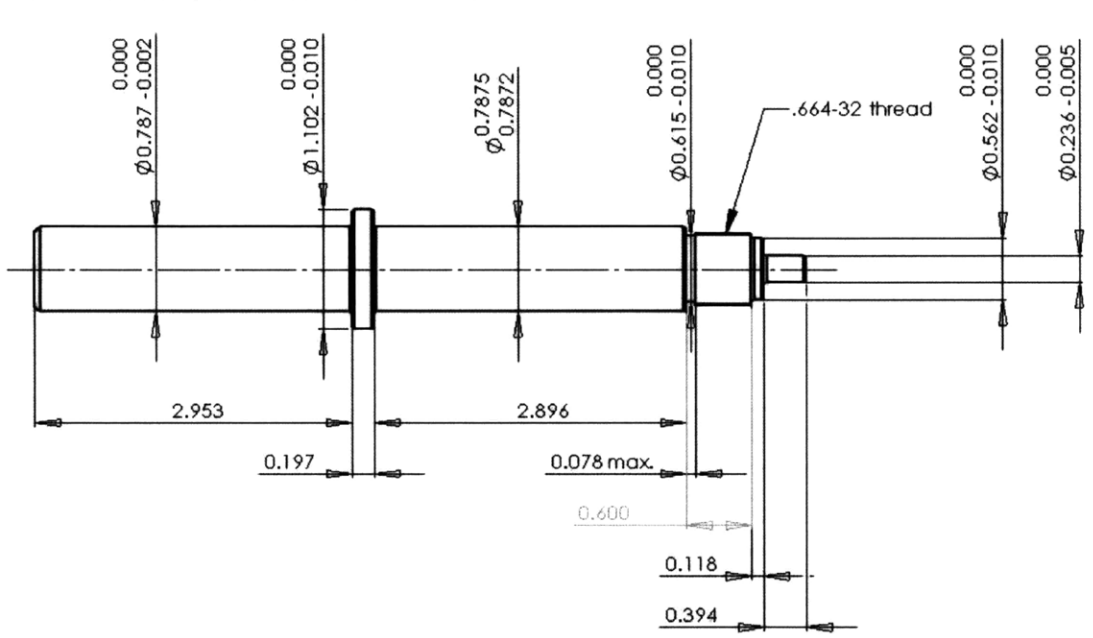

UNLESS OTHERWISE SPECIFIED:
All dimensions in inches
Tolerances are ±0.005

MATERIAL: Steel

SURFACE FINISH: 16 µ in

TITLE:
Shaft (Side View)

Contact: Miguel Saez masaez@mit.edu

SCALE: 1:1

SHEET 1 OF 3

5 4 3 2 1

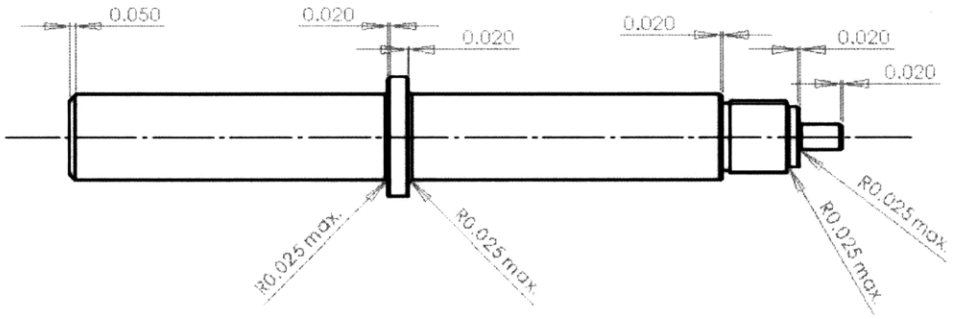

Note: All chamfers are 45° unless otherwise specified.

UNLESS OTHERWISE SPECIFIED:	
All dimensions in inches	
Tolerances are	±0.005
MATERIAL:	Steel
SURFACE FINISH:	16 μ in

TITLE:
Shaft (Side View)
Chamfer and Radius Locations

Contact: Miguel Saez masaez@mit.edu

SCALE: 1:1 SHEET 2 OF 3

5 4 3 2 1

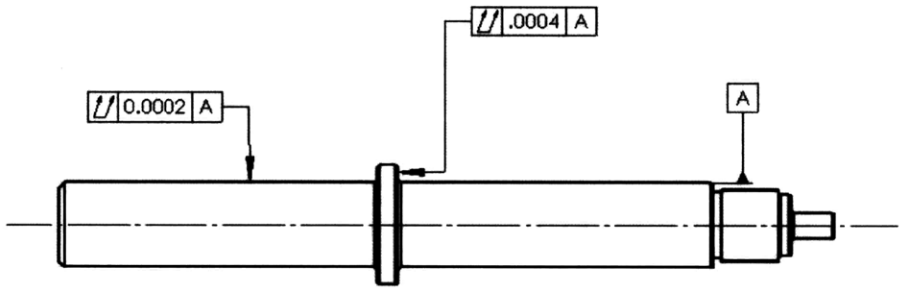

UNLESS OTHERWISE SPECIFIED:
All dimensions in inches
Tolerances are ±0.005
MATERIAL: Steel
SURFACE FINISH: 16 μ in

Contact: Miguel Saez masaez@mit.edu

TITLE:
Shaft (Side View)
Form Tolerances

SCALE: 1:1 SHEET 3 OF 3

5 4 3 2 1

Bibliography

[1] Nanotechnologies for the textile market. Technical report, Cientifica Ltd., 2006.

[2] P. A. Anquetil. *Large Contraction Conducting Polymer Molecular Actuators.* PhD thesis, Massachusetts Institute of Technology, 2004.

[3] W. J. Bae. Cortical recording with conducting polymer electrodes. Master's thesis, Massachusetts Institute of Technology, 2008.

[4] M. Bayindir, F. Sorin, A. F. Abouraddy, J. Viens, S. D. Hart, J. D. Joannopoulos, and Y. Fink. Metal-insulator-semiconductor optoelectronic fibres. *Nature*, 431:826–829, 2004.

[5] M. F. Bear, B. W. Connors, and M. A. Paradiso. *Neuroscience: Exploring the Brain.* Lippincott Williams & Wilkins, 3rd edition, 2007.

[6] D. Bowman and B.R. Mattes. Conductive fibre prepared from ultra-high molecular weight polyanaline for smart fabric and interactive textile applications. *Synthetic Metals*, 154:29–32, 2005.

[7] F. Carpi and D. De Rossi. Electroactive polymer-based devices for e-textiles in biomedicine. *IEEE Trans. Inf. Technol. Biomed.*, 9(3):295–318, 2005.

[8] V. M. Cepak and C. R. Martin. Preparation of polymeric micro- and nanostructures using a template-based deposition method. *Chem. Mater.*, 11:1363–1367, 1999.

[9] K.C. Cheung. Implantable microscale neural interfaces. *Biomedical Microdevices*, 9:923–938, 2007.

[10] C. K. Chiang, C. R. Fincher Jr., Y. W. Park, A. J. Heeger, H. Shirakawa, E. J. Louis, S. C. Gau, and A. G. MacDiarmid. Electrical conductivity in doped polyacetylene. *Phys. Rev. Lett.*, 39(17):1098–1101, 1977.

[11] I. S. Chronakis, S. Grapenson, and A. Jakob. Conductive polypyrrole nanofibers via electrospinning: Electrical and morphological properties. *Polymer*, 47:15971603, 2006.

[12] National Instruments Corporation. http://www.ni.com/labview/.

[13] S. Coyle, Y. Wu, K. Lau, D. De Rossi, G. Wallace, and D. Diamond. Smart nanotextiles: A review of materials and applications. *MRS Bulletin*, 32(5):434–442, 2007.

[14] T. A. Fofonoff. *Fabrication and Use of Conducting Polymer Linear Actuators.* PhD thesis, Massachusetts Institute of Technology, 2008.

[15] T.A. Fofonoff, S. M. Martel, N. G. Hatsopoulos, J. P. Donoghue, and I. W. Hunter. Microelectrode array fabrication by electrical discharge machining and chemical etching. *IEEE Trans. Biomed. Eng.*, 51(6):890–895, 2004.

[16] J. Foroughi, G. M. Spinks, G. G. Wallace, and P. G. Whitten. Production of polypyrrole fibres by wet spinning. *Synthetic Metals*, 158:104–107, 2008.

[17] The Nobel Foundation. http://nobelprize.org/index.html.

[18] A. G. Green and A. E. Woodhead. Aniline-black and allied compounds. part i. *J. Chem. Soc., Trans.*, 97:2388–2403, 1910.

[19] N. K. Guimard, N. Gomez, and C. E. Schimdt. Conducting polymers in biomedical engineering. *Progress in Polymer Science*, 32:876–921, 2007.

[20] T. A. Harris and M. N. Kotzalas. *Rolling Bearing Analysis.* CRC Press, 5th edition, 2006.

[21] T. Ito, H. Shirakawa, and S. Ikeda. Simultaneous polymerization and formation of polyacetylene film on the surface of concentrated soluble ziegler-type catalyst solution. *J. Polym. Sci., Poly. Chem. Ed.*, 12:11–20, 1974.

[22] J. N. Juang. *Applied System Identification.* Prentice Hall, Englewood Cliffs, NJ, 1994.

[23] Y. K. Kim and A. F. Lewis. Concepts for energy-interactive textiles. *MRS Bulletin*, 28(8):592–596, 2003.

[24] H. Letheby. On the production of a blue substance by the electrolysis of sulfate of aniline. *J. Chem. Soc.*, 15:161–163, 1862.

[25] R. R. Llinas, K. D. Walton, M. Nakao, I. W. Hunter, and P. A. Anquetil. Neurovascular central nervous recording/stimulating system: Using nanotechnology probes. *J. Nanopart. Res.*, 7:111–127, 2005.

[26] C. Luo and A. Chakraborty. Effects of dimensions on the sensitivity of a conducting polymer microwire sensor. *Microelectron. J.*, 2009. In press.

[27] A. G. MacDiarmid, W. E. JonesJr., I. D. Norris, J. Gao, A. T. Johnson Jr., N. J. Pinto, J. Hone, B. Han, F. K. Ko, H. Okuzaki, and M. Llaguno. Electrostatically-generated nanofibers of electronic polymers. *Synthetic Metals*, 119:27–30, 2001.

[28] J. Madden. *Conducting Polymer Actuators.* PhD thesis, Massachusetts Institute of Technology, 2000.

[29] P. Madden. *Development and Modeling of Conducting Polymer Actuators and the Fabrication of a Conducting Polymer Based Feedback Loop.* PhD thesis, Massachusetts Institute of Technology, 2003.

[30] J. M. Mativetsky and W. R. Datars. Morphology and electrical properties of template-synthesized polypyrrole nanocylinders. *Physica B*, 324:191204, 2002.

[31] B. J. Muro, J. R. Steele, T. E. Campbell, and G. G. Wallace. Wearable textile biofeedback systems: Are they too intelligent for the wearer? In *Proc. Int. Workshop New Generation Wearable Syst. for e-Health: Toward Revolution of Citizens Health, Life Style Management*, pages 187–193, 2003.

[32] E. Oberg, F. D. Jones, H. L. Horton, and H. H. Ryffel. *Machinery's Handbook.* Industrial Press, New York, New York, 28th edition, 2008.

[33] P. V. Pillai. Conducting polymer actutaor enhancement through microstructuring. Master's thesis, Massachusetts Institute of Technology, 2007.

[34] P. V. Pillai and I. W. Hunter. Stochastic system identification of the compliance of conducting polymers. In *Mater. Res. Soc. Symp. Proc.*, volume 1134. Mater. Res. Soc., 2009.

[35] R. Z. Pytel. *Artificial Muscle Morphology Structure/Property Relationships in PPy Actuators.* PhD thesis, Massachusetts Institute of Technology, 2007.

[36] S. Roth. *One-dimensional Metals.* Springer-Verlag, 1995.

[37] B. P. Ruddy. Conducting polymer wires for intravascular neural recording. Master's thesis, Massachusetts Institute of Technology, 2006.

[38] B. Schmid. Characterization of macro-length conducting polymers and the development of a conducting polymer rotary motor. Master's thesis, Massachusetts Institute of Technology, 2005.

[39] H. L. Schreuder-Gibson, Q. Truong, J. E. Walker, J. R. Owens, J. D. Wander, and W. E. Jones Jr. Chemical and biological protection and detection in fabrics for protective clothing. *MRS Bulletin*, 28(8):592–596, 2003.

[40] E.P. Scilingo, F. Lorussi, A. Mazzoldi, and D. De Rossi. Strain-sensing fabrics for wearable kinaesthetic-like systems. *IEEE Sensors J.*, 3(4):460–467, 2003.

[41] SKF USA Inc. *Bearing Installation and Maintenance Guide*, 2001.

[42] T. A. Skotheim, R. L. Elsenbaumer, and J. R. Reynolds, editors. *Handbook of Conducting Polymers.* Marcel Dekker, 2nd edition, 1998.

[43] G. M. Spinks, V. Mottaghitalab, M. Bahrami-Samani, P. G. Whitten, and G. G. Wallace. Carbon-nanotube-reinforced polyaniline fibers for high-strength artificial muscles. *Advanced Materials*, 18:637–640, 2006.

[44] J. Tsukamoto, A. Takahashi, and K. Kawasaki. Structure and electrical properties of polyacetylene yielding a conductivity of 105 s/cm. *Jpn. J. Appl. Phys.*, 29(1):125–130, 1990.

[45] N. Vandesteeg. *Synthesis and Characterization of Conducting Polymer Actuators.* PhD thesis, Massachusetts Institute of Technology, 2006.

[46] N. S. Wiedenman. *Towards Programmable Materials Tunable Material Properties Through Feedback Control of Conducting Polymers.* PhD thesis, Massachusetts Institute of Technology, 2008.

[47] M. Yamaura, T. Hagiwara, and K. Iwata. Enhancement of electrical conductivity of ppy film by stretching-counter ion effect. *Synthetic Metals*, 26(3):209–224, 1988.

[48] X. Zhang, Z. L, M. Wen, H. Liang, J. Zhang, and Z. Liu. Single-walled carbon nanotube-based coaxial nanowires: Synthesis, characterization, and electrical properties. *J. Phys. Chem. B*, 109(3):1101–1107, 2005.